micro

MDPI

Review

Antimicrobial Efficacy of Silver Nanoparticles: Synthesis Routes, Structure–Activity Relationships and Recent Advances in Plant-Mediated Green Synthesis

Abderrahmen Merghni [1,*], Molka Mrabet [2] and Faouzi Ayari [2]

[1] Laboratory of Antimicrobial Resistance LR99ES09, Faculty of Medicine of Tunis, University of Tunis El Manar, Tunis 1007, Tunisia
[2] Laboratory of Chemical, Galenic & Pharmacological Drug Development-LR12ES09, Faculty of Pharmacy of Monastir, University of Monastir, Avicenne Street, Monastir 5000, Tunisia
* Correspondence: abderrahmen.merghni@fmt.utm.tn

Abstract

Silver nanoparticles (Ag-NPs), typically sized between 1 and 100 nm, hold considerable promise in biomedicine. Owing to their broad biological activity—most notably their antibacterial action against drug-resistant bacteria—a growing number of research efforts are now directed toward the most environmentally friendly routes for Ag-NP synthesis. Ag-NPs can be prepared through chemical, physical or biological approaches. The chemical route is inexpensive and gives a high yield, but relies on reducing agents and stabilisers that carry a risk of toxicity. Physical methods avoid these chemicals—using a radiation beam as the reducing agent instead—but are energy-intensive and require specialised equipment. These drawbacks have progressively shifted research toward green biosynthesis. In this review, we summarise recent progress in the synthesis of Ag-NPs by physical, chemical and biological approaches and discuss their antimicrobial properties, with particular attention paid to the green synthesis of Ag-NPs from plant-derived (including plant-waste) extracts. Unlike earlier overviews, we compare the three families of methods against the same criteria (control of size and shape, scalability, environmental burden and suitability for biomedical use), relate particle properties to antimicrobial performance, and treat toxicity and bacterial silver resistance in dedicated sections. We further highlight developments published between 2023 and 2026 and outline the main challenges—toxicity, standardisation and scale-up—that will determine whether Ag-NPs can be translated into clinically and industrially viable antimicrobial agents.

Keywords: silver nanoparticles; physical synthesis; chemical synthesis; green synthesis; antimicrobial efficacy; antimicrobial resistance; structure–activity relationship; toxicity; silver resistance

Check for updates

Received: 18 September 2026
Revised: 10 October 2026
Accepted: 21 October 2026
Published: 27 October 2026

Copyright: © 2026 by the authors. Licensee MDPI, Basel, Switzerland. This article is an open access article distributed under the terms and conditions of the Creative Commons Attribution (CC BY) license.

1. Introduction

Silver (Ag, atomic number 47) is a transition metal belonging to the so-called "noble" group. It is a comparatively rare element—with an average crustal abundance of about 0.1 ppm and a soil concentration of about 0.3 ppm [1]—that occurs naturally both as the pure, ductile white metal and within ores. Silver has a long history of medicinal use: modern microbiological and pharmacological research has largely validated centuries-old practices that relied on its antimicrobial properties. Metallic silver (Ag^0) has been used in surgical prostheses, silver salts have been instilled as eye drops in newborns to prevent

gonorrhoea-associated blindness, and silver-based formulations have been employed in dental practice and in the management of dental hypersensitivity and periapical infections [2,3]. More broadly, silver shows activity against Gram-positive and Gram-negative pathogenic bacteria [2,4], against mycotoxigenic and pathogenic fungal strains [5], and against several respiratory viruses, including SARS-CoV-2 [6,7].

Silver nanoparticles represent another, increasingly important form of silver used across biological, biomedical and pharmaceutical technologies, and they are now being revisited as an alternative to conventional antibiotics. From a market standpoint, the global Ag-NP market was valued at USD 1.5 billion in 2020 and was projected to reach USD 6.6 billion by 2030, corresponding to a compound annual growth rate (CAGR) of 15.6% over 2021–2030 [8]; more recent industry estimates published in 2024–2025 continue to project sustained growth, driven chiefly by demand for antimicrobial materials in healthcare and by the expansion of printed and flexible electronics [9]. With the advance of nanotechnology, silver salts are also used as precursors for the synthesis of Ag-NPs, which are aggregates or agglomerates typically 1–100 nm in size [10]. Ag-NPs display efficient antiviral action against severe acute respiratory syndrome coronavirus-2 (SARS-CoV-2) [7], together with well-documented antimicrobial efficacy [4,10].

Ag-NPs are most commonly produced by chemical reduction, in which a silver salt (typically $AgNO_3$) is reduced by an agent such as sodium borohydride or sodium citrate to yield colloidal Ag-NPs of controllable size and shape [11]. Physical approaches, by contrast, generate ligand-free Ag-NPs without any chemical reagent, although this comes at the cost of high-energy consumption and specialised equipment [12]. Finally, green or biological syntheses rely on plant extracts, bacteria, fungi or polysaccharides as reducing and capping agents; they offer eco-friendly, scalable routes with generally good biocompatibility, albeit with broader particle-size distributions [10].

As is already well established, the size, shape and surface morphology of Ag-NPs depend largely on the synthesis method used. In this review, we discuss recent developments in the synthesis of Ag-NPs by physical, chemical and biological methods, and we examine how biosynthesized Ag-NPs, in particular, contribute to antimicrobial applications relevant to public health and to the prevention of infectious disease.

Several reviews of Ag-NP green synthesis and antimicrobial activity have appeared in recent years [10,13–17]. Most are organised around the biological source (plants, bacteria, fungi, algae) or around a single application, and they usually treat physical and chemical routes only as a point of reference. The present review takes a different angle. We place physical, chemical and plant-mediated routes side by side and judge them by the same practical criteria: how well each controls particle size and shape, whether it can realistically be scaled up, what it costs in energy and reagents, and whether the product is suited to biomedical or food-contact use (Section 7.5). We then ask how the properties these routes give to the particles translate into antimicrobial activity (Section Linking Physicochemical Properties to Antimicrobial Performance), which of the proposed mechanisms rest on direct experimental evidence and which remain hypotheses (Section 4), and what is known about toxicity, environmental fate and bacterial silver resistance (Sections 4.2 and 8). Plant-mediated synthesis, including from agro-food waste, is treated in more depth than the other routes, with emphasis on the chemistry of Ag^+ reduction and on how extract composition shapes the final material (Section 7).

Literature Search Strategy

The literature was collected from Web of Science Core Collection, Scopus, PubMed and Google Scholar. Searches combined “silver nanoparticles” or “AgNPs” with “antibacterial”, “antimicrobial”, “green synthesis”, “plant extract”, “laser ablation”, “chemical

reduction", "photoreduction", "sonochemical" and "microwave", and, for Sections 4 and 8, with "toxicity", "cytotoxicity" and "silver resistance". Foundational work on synthesis and mechanisms was not restricted by date, whereas the studies used to illustrate each synthesis route were drawn mainly from 2017 to 2026, with particular attention to 2023–2026 for the recent developments highlighted here. We kept original research articles and reviews in English that described the synthesis route and reported at least one antimicrobial or toxicological end point. We excluded papers in which Ag-NPs were used only as catalysts, sensors or electronic materials, papers without any characterisation of the particles, conference abstracts and preprints. The reference lists of the retrieved reviews were screened to trace earlier primary sources. This is a narrative review, not a systematic one, and no quantitative pooling was attempted, although the search was documented along the lines of the PRISMA 2020 recommendations [18]. Because the evidence is heterogeneous (different strains, inocula, assays and dose metrics), results from different studies are compared qualitatively.

2. Silver Metal Properties

Humans are continuously exposed to low levels of silver, mainly through food and drinking water and, to a lesser extent, air; the resulting daily intake can reach 20–80 μg [1]. However, only about 10% of ingested silver is absorbed, the remainder being excreted via the intestine [1]. Once absorbed, Ag^0 can be ionised to release the biologically active Ag^+ species; the solubility of the resulting silver salts depends strongly on the nature of the counter-ion (Table 1).

Table 1. Solubility of common silver salts in water at 298.15 K [1,19].

Silver Salt	Solubility in H_2O (g L^{-1})	K_s
$AgNO_3$	1220	-
CH_3COOAg	10.2	1.94×10^{-3}
AgOH *	Insoluble	1.52×10^{-8}
AgCl	Insoluble	1.77×10^{-10}
AgBr	Insoluble	5.35×10^{-13}
AgI	Insoluble	8.52×10^{-17}
Ag_3AsO_4	Insoluble	1.03×10^{-22}
Ag_2S	Insoluble	6.3×10^{-50}
Ag_2Se	Insoluble	1.0×10^{-53}

* Unstable; tends to convert into insoluble Ag_2O.

As Table 1 shows, Ag_2S and Ag_2Se are the least soluble—and thus the most chemically inert and least hazardous—silver compounds. However, once ingested, the hydrochloric acid present in gastric fluid (together with K^+, Cl^- and Na^+, Cl^- ions) converts silver compounds into crystalline AgCl, and subsequently into the soluble and comparatively toxic $[AgCl_2]$-complex [1]. The situation differs for silver nanoparticles: upon ingestion, gastric HCl (~0.1 M) partially converts metallic silver into Ag^+ and then into AgCl(cr) [1,20], while the undissolved fraction of Ag-NPs proceeds into the intestine and the bloodstream, from where it is either translocated throughout the body or excreted [20].

3. Synthesis and Characterisation of Ag-NPs

The widespread use of Ag-NPs—a consequence of their distinctive textural properties—has raised legitimate questions about their potential toxicity to humans, an issue that is closely tied to the preparation method employed [21]. Ag-NPs can be obtained through physical, chemical or biological routes, which yield nanomaterials that differ markedly in structure, surface morphology, physicochemical properties and bioactivity [10,22]. These methods fall broadly into two categories (Figure 1):

- Top-down approach: bulk silver is subjected to an external force (a beam, a ray, etc.) that breaks it down into nanostructures;
- Bottom-up approach: synthesis starts from Ag^+ ions, which are progressively reduced and assembled into Ag-NPs until the desired size and shape are reached [22,23].

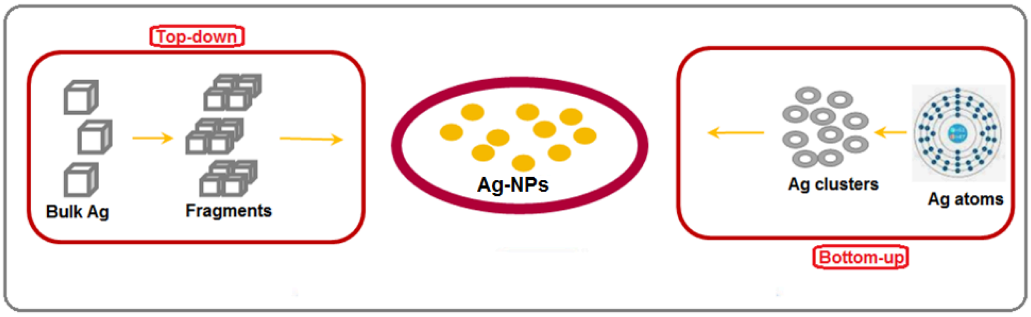


Figure 1. The two principal approaches used for the synthesis of Ag-NPs (adapted from [22]).

Ag-NPs are used in surgical coatings and in cosmetic formulations owing to their antimicrobial properties, which are closely related to particle size and dose. For example, Agnihotri et al. [4] prepared size-controlled Ag-NPs (5–100 nm) using a two-stage thermal-treatment protocol and found that 5 nm particles inhibited the growth of *Escherichia coli* (*E. coli*, MTCC 443) within one hour, whereas 7 nm and 10 nm particles took roughly twice as long. The authors concluded that smaller Ag-NPs display greater bactericidal activity because their surface-area-to-volume ratio is larger. A range of complementary techniques has since been used to elucidate the size distribution, morphology, textural properties and colloidal stability of Ag-NPs; the most widely used of these are summarised in Table 2.

Table 2. Main techniques used to characterise Ag-NPs [24].

Technique	Abbreviation	Information Provided
Atomic force microscopy	AFM	Size and shape
Dynamic light scattering	DLS	Hydrodynamic size distribution
Energy-dispersive X-ray spectroscopy	EDX	Elemental surface composition
Fourier-transform infrared and Raman spectroscopy	FTIR/Raman	Structure and functional groups
Magic-angle-spinning nuclear magnetic resonance	MAS-NMR (^{109}Ag)	Coordination environment of Ag
Near-field scanning optical microscopy	NSOM	Size and shape
Scanning electron microscopy	SEM	Size distribution and shape of particles/aggregates
Transmission electron microscopy	TEM	Size distribution and shape at the nanoscale
X-ray diffraction	XRD	Crystalline phase
X-ray photoelectron spectroscopy	XPS	Elemental surface composition and oxidation state
Zeta potential	ZP	Colloidal stability (surface charge)

Linking Physicochemical Properties to Antimicrobial Performance

No single technique in Table 2 describes a nanoparticle sample well enough to explain its biological behaviour, because the techniques measure different things. TEM and SEM give the size of the metallic core in the dry state. DLS reports a hydrodynamic diameter that includes the capping layer and any aggregates, and it is biased towards the larger particles in a polydisperse sample. The UV-Vis plasmon band is a quick but indirect indicator of size, shape and aggregation. XRD and XPS establish the crystalline phase and the oxidation state of silver at the surface, which matters because partly oxidised or sulfidised surfaces release Ag^+ differently from clean metallic ones. Zeta potential describes the surface charge in the medium used for the measurement, not necessarily in the broth or agar in which bacteria are later exposed. A sample is only adequately described when core size (TEM), hydrodynamic size and aggregation state in the actual test medium (DLS), surface chemistry (FTIR, XPS, zeta potential) and the amount of dissolved silver (typically by ICP-MS or atomic absorption after ultrafiltration) are reported together. Many of the studies discussed in Sections 5–7 report only one or two of these parameters, which is one reason why the values in the tables of this review cannot simply be ranked against each other.

Within that limitation, a few relationships are reasonably well established. Particle size matters because smaller particles expose more surface per unit mass, dissolve faster and can approach the cell envelope more closely. The 5 nm particles of Agnihotri et al. [4] acted faster on *E. coli* than 7 and 10 nm particles, and Morones et al. [25] observed that particles of roughly 1–10 nm attached to the membrane of Gram-negative bacteria. The same trend appears for laser-ablated particles, where Hamid et al. [26] linked laser energy, and therefore size, to antibacterial potency. Size is rarely the whole story, however, since the capping layer also contributes, as discussed below.

Shape matters through the crystal facets that are exposed. Pal et al. [27] compared truncated triangular nanoplates, spheres and rods against *E. coli* and found the triangular plates, rich in {111} facets, to be the most active at the lowest silver content. This is a single-species comparison between particles made by different routes and should not be generalised, but it fits the idea that reactive facets count as much as total surface area. For the nanocubes, nanowires and other shapes mentioned in Section 6.1, antimicrobial data are still scarce.

Surface charge and capping agents govern colloidal stability and the way particles approach the cell. Bacterial surfaces are generally negatively charged, so strongly negative particles (the citrate-capped ones that dominate the chemical-reduction examples discussed in Section 6) may be partly repelled, whereas positively charged capping agents such as chitosan or quaternary surfactants promote contact; the same coatings also change how fast Ag^+ is released. Aggregation cancels much of the benefit of small size. In biological media, chloride, phosphate, thiols and proteins react with the particle surface, so that a nominal 10 nm suspension in water may behave quite differently once it is placed in broth [28]. Dissolution is the other variable. Ag-NPs oxidise in oxygenated water and release Ag^+ over hours to days, at a rate that depends on size, capping, temperature, pH and the presence of ligands [29], and stored suspensions can become more toxic with time as their ion content increases [30]. A result obtained on a fresh sample and one obtained after storage may therefore reflect different amounts of dissolved silver, even for the same batch.

The assay itself also shapes the numbers. The disc-diffusion data in Table 3 depend on how fast particles diffuse through agar, which is slower for large or aggregated particles, so inhibition zones are a poor measure of intrinsic potency. Broth microdilution (MIC and MBC) and time-kill assays are better suited, provided that the medium composition is reported and its interaction with silver is considered. For this reason, the comparisons

between physical, chemical and plant-based routes in this review are qualitative, and the figures in the tables are best read as examples rather than as rankings.

Table 3. Inhibition-zone diameters (mm) for Ag-NPs against selected bacteria [31].

Group	Strain	0.25 mg mL^{-1}	0.5 mg mL^{-1}	1 mg mL^{-1}
Gram-positive	*Staphylococcus aureus*	17	18	19
Gram-positive	*Bacillus cereus*	16	18	19
Gram-positive	*Bacillus luteus* (in-house strain)	20	21	24
Gram-positive	*Bacillus subtilis*	16	17	19
Gram-positive	*Listeria monocytogenes*	16	17	18
Gram-negative	*Escherichia coli*	17	18	21
Gram-negative	*Pseudomonas aeruginosa*	23	24	26
Gram-negative	*Klebsiella pneumoniae*	16	18	19
Gram-negative	*Proteus vulgaris*	13	14	18

4. Mode of Action of Ag-NPs Against Bacterial Cells

The antimicrobial activity of Ag-NPs is most commonly assessed by the agar disc-diffusion method. Cakić et al. [31], for instance, prepared bacterial suspensions directly from plate colonies, suspended them in 5 mL of sterile 0.85% saline, and adjusted turbidity to the 0.5 McFarland standard (~10^8 CFU mL^{-1}). Ten-fold serial dilutions were then inoculated onto tryptone soya agar plates. Sterile 9 mm cellulose discs impregnated with 0.25, 0.5 and 1 mg mL^{-1} Ag-NP suspensions were applied to the plates, which were incubated for 24 h at 310 K (37 °C). The resulting inhibition-zone diameters are summarised in Table 3.

Several complementary mechanisms have been proposed to explain the antibacterial activity of Ag-NPs (Figure 2) [5]:

(1) Disruption of the cell wall and cytoplasmic membrane: silver ions (Ag^+) released from Ag-NPs adhere to, and can penetrate, these structures.
(2) Ribosome denaturation: silver ions denature ribosomes, thereby inhibiting protein synthesis.
(3) Inhibition of ATP synthesis: silver ions inactivate the respiratory enzymes of the cytoplasmic membrane, halting adenosine triphosphate (ATP) production.
(4) Oxidative membrane damage: disruption of the electron-transport chain generates reactive oxygen species (ROS) that further damage the cell membrane.

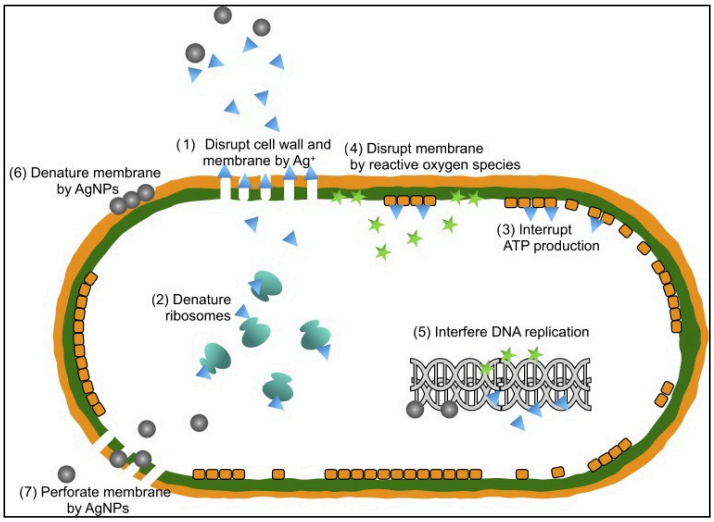


Figure 2. Principal antibacterial mechanisms of silver nanoparticles, adapted from Yin et al. [6].

4.1. What Is Supported by Experiment and What Is Not

The mechanisms listed above are often presented side by side as if they carried equal weight, but the experimental support behind them is uneven. The evidence is strongest for the interaction of silver with the cell envelope. Electron microscopy of *E. coli* exposed to Ag-NPs shows pits in the cell wall and accumulation of particles in the membrane [32], and similar damage is produced by silver ions [33]. Effects on ribosomes and protein synthesis have mostly been demonstrated with silver ion solutions: in *E. coli* treated with Ag^+, ribosome integrity and the expression of envelope and ATP-related proteins were affected [34], but there is little direct evidence that intact nanoparticles do the same inside the cell. Inhibition of respiratory enzymes and loss of ATP are consistent with the high affinity of Ag^+ for thiol groups [33] and are therefore probably, at least in part, ionic effects. ROS formation is reported in many studies, usually with fluorescent probes such as DCFH-DA, which are not specific and respond to other changes in cell redox state; whether ROS drive cell death or are a consequence of respiratory damage is still unresolved. Items 2 and 3 of the list should thus be regarded as well supported for Ag^+ and as plausible but largely unproven for the particle itself, while item 4 is an observation whose causal role remains uncertain.

The relative weight of dissolved Ag^+ and of the particle surface is the central open question. Xiu et al. [35] prevented oxidative dissolution by working under anaerobic conditions and found that particles of several sizes and coatings had negligible activity against *E. coli*, whereas the same particles became toxic once oxygen was admitted and Ag^+ formed; they concluded that the activity of Ag-NPs is largely explained by the ions they release. Others have argued for a particle-specific component, for instance when particles adhere to the cell envelope and create a high local concentration of Ag^+ [25,32]. A pragmatic reading is that dissolution is necessary for most of the activity of the Ag-NPs discussed in this review, while the particle acts as a reservoir and sometimes as a carrier that raises the local dose. Which of the two dominates probably depends on size, capping, medium and species, and the question can only be settled when studies report dissolved silver alongside the biological read-out, ideally with an Ag^+ control at the same total silver content.

4.2. Bacterial Adaptation and Silver Resistance

Resistance to silver is not a theoretical concern, and it affects how the activity data in the following sections should be read. Determinants of silver resistance have been known for decades: the *sil* genes, first described on a plasmid from a *Salmonella* isolate from a hospital burns unit, encode an efflux system (SilCBA, SilP) and a periplasmic silver-binding protein (SilE) that confer resistance to Ag^+ [36]. Adaptation to nanoparticulate silver has also been shown in the laboratory. *Bacillus* sp. adapted to nanosilver after repeated exposure [37], and Panáček et al. [38] reported that *E. coli* and *P. aeruginosa* strains became resistant to Ag-NPs after serial passage by producing flagellin, which makes the particles aggregate and so lowers the concentration of active silver. The link between genotype and phenotype is not straightforward: surveys of Gram-negative isolates found *sil* genes in strains that were not resistant and resistance in strains that lacked them [39].

Sub-lethal exposure, which is the situation created by slow release from coated surfaces or by silver in the environment, is where the risk is greatest. Most of the studies in Sections 5–7 report activity after a single, short exposure and do not test for adaptation, so their results say little about how durable the effect is. We come back to the implications for clinical and food-safety uses in Sections 8 and 9.

5. Antibacterial Activity of Ag-NPs Obtained by Physical Methods

Physical methods (the top-down approach, Figure 1) produce a uniform and evenly distributed layer of Ag-NPs on a substrate surface and/or embedded within an (in)organic matrix. These methods rely on the interaction of a radiation beam (gamma, X-ray, UV, electron, etc.) with metallic silver or a silver precursor, and include the following main techniques.

5.1. Laser Ablation (LA)

In this green method, a laser beam ablates the surface layers of bulk silver with high spatial precision. LA can be carried out in various media—air, vacuum or liquid [22]—although pulsed LA in liquid medium (LALM) is by far the most widely used configuration for nanoparticle fabrication [40]. A typical LALM setup comprises a focusing lens, a high-power pulsed laser, a liquid-filled container, a stirrer and a linear positioner: the metal target is submerged in liquid, and a Nd:YAG pulsed laser beam (532 nm or 1064 nm) ablates the plate [22,23].

Ag-NPs obtained by LA display significant biological activity and are increasingly explored for antimicrobial applications. In aqueous medium, Fernández-Arias et al. [41] used two Nd:YVO_4 laser sources (14 ns pulses at 532 nm, and 20 ns pulses at 1064 nm) and obtained crystalline, rounded nanoparticles with a bimodal size distribution (18.11–21.56 nm and 13.40–14.39 nm). The resulting materials showed significant antibacterial activity against *Staphylococcus aureus* (*S. aureus*), with bacterial growth markedly reduced after 13 h; re-irradiating the samples further improved their antibacterial performance. Similarly, Ag-NPs prepared by femtosecond pulsed LA in organic (THF, DMF) and inorganic (double-distilled and deionized water) solvents [42] showed potent activity against both Gram-negative (*Pseudomonas aeruginosa*, *P. aeruginosa*; *E. coli*) and Gram-positive (*Bacillus subtilis*, *B. subtilis*; *S. aureus*) strains.

In a review, Nene et al. [21] described the preparation of Ag-NPs by LA and highlighted their strong antibacterial, antifungal and antiviral potential once particle size is kept below 100 nm. Ruiz et al. [43] synthesised Ag-NPs in pure water by nanosecond pulsed LA, obtaining particles with an average size of 10.17 ± 2.95 nm. At concentrations of 100 and 250 μg mL^{-1}, tested against *S. aureus* at two inoculum densities (10^3 and 10^5 CFU mL^{-1}) over 24 h, the 100 μg mL^{-1} samples showed early bacteriostatic activity that did not persist, whereas the 250 μg mL^{-1} samples were both bactericidal and bacteriostatic.

Using the same technique, Pérez-Tanoira et al. [44] evaluated bacterial adhesion and biofilm formation by *S. aureus* and by a mixed oral flora comprising *Streptococcus oralis*, *Actinomyces naeslundii*, *Veillonella dispar* and *Porphyromonas gingivalis*. Ag-NPs prevented biofilm formation by both *S. aureus* and the mixed oral flora, with the strongest effect observed for nanoparticles re-irradiated three times.

Laser ablation has continued to attract interest for its simplicity, speed and eco-friendliness. It has been used to generate Ag-NPs of varying sizes for the treatment of bacterial dental caries caused by *Streptococcus mutans* (*S. mutans*) [45], against *E. coli* in food-packaging applications [46], and even for the remediation of dye-contaminated water [47]. More recently, Hamid et al. [26] compared Ag-NPs produced by pulsed laser ablation at different laser energies and confirmed a clear, energy-dependent relationship between particle size and antibacterial potency against *Staphylococcus aureus* and *Klebsiella pneumoniae*, reinforcing the case for LA as a reagent-free, tunable route to antibacterial Ag-NPs.

5.2. Chemical Vapour Deposition (CVD) and Atomic Layer Deposition (ALD)

Both techniques require vacuum conditions and high temperatures. CVD proceeds through: (i) thermal decomposition of a volatile silver precursor, e.g., $Ag_5(O_2CC_2F_5)_5(H_2O)_3$ [48];

(ii) transport of the resulting metal vapour to the reactor chamber; (iii) adsorption of the vapour onto the substrate surface and formation of intermediate species; and (iv) decomposition of these intermediates on the heated substrate, followed by nucleation and growth of the solid layer and removal of volatile by-products via the carrier gas [12].

ALD, by contrast, deposits uniform, conformal nanolayers through alternating, self-limiting exposures of the substrate to two precursor vapours [12], and includes (i) thermal ALD, as used by Mäkelä et al. [49] with [Ag(2,2-dimethyl-6,6,7,7,8,8,8-heptafluoro-3,5-octanedionato)(PEt_3)] and $BH_3(NHMe_2)$ at 383 K; (ii) plasma-enhanced ALD, as used by Wack et al. [50] with the same precursor and H_2 at 373 K; and (iii) direct-liquid-injection ALD, as used by Devin-Mullin et al. [51] with [Ag(1,1,1,5,5,5-hexafluoroacetylacetonato)(1,5-cyclooctadiene)] and propan-1-ol at 383–423 K.

Gerullis et al. [52] used atmospheric-pressure plasma CVD to deposit Ag-NPs on SiO_2 and evaluated their antibacterial activity against *E. coli* HB101 using the BacTiter-Glo assay, along with promising antimycotic activity against mould strains such as *Aspergillus niger*. In 2022, Astaneh et al. [53] investigated silver-containing N95 filter masks, depositing Ag-NPs by ALD (1100–1500 cycles at 363–393 K) using the same fluorinated precursor together with $BH_3(NHMe_2)$ at 369 K; the resulting materials were effective against the airborne pathogen *S. aureus*. Nazarov et al. [54] synthesised Ag-NPs supported on ALD-grown TiO_2 coatings (using $TiCl_4$ as the titanium precursor and hydrogen plasma as reducing agent) and systematically varied reactor temperature, precursor sublimation temperature, pulse timing and cycle number to optimise growth; the resulting materials showed promising antibacterial activity against *S. aureus*.

Notably, relatively few studies between 2018 and 2023 addressed CVD/ALD routes to antibacterial Ag-NPs, despite the fine control over growth conditions that these techniques afford—a gap that still represents an opportunity for future work.

5.3. Plasma-Assisted Synthesis

Plasma-discharge synthesis, with or without stabilisers, is an environmentally friendly, fast and economical route to Ag-NPs. Chandana et al. [55] produced (un)supported Ag-NPs using an atmospheric-pressure plasma jet under ambient conditions, without any reducing agent or stabiliser: an $Ag^+NO_3^-$ solution (1–3 mM) was exposed to a plasma jet positioned about 3 mm above the liquid surface for 5–15 min. Particle size (11–16 nm) was tuned by adjusting the reaction conditions and confirmed by XRD, TEM and UV-Vis/fluorescence spectroscopy. Against *E. coli* strains DH5-alpha, BL21 and K-12, bacterial growth was delayed at low Ag-NP concentrations (10–50 mg L-1) and fully inhibited at higher concentrations (up to 40 g L^{-1}). Using room-temperature atmospheric-pressure microplasma, Sun et al. [56] prepared bare and chitosan-supported Ag-NPs whose size distribution depended on precursor concentration; the resulting Ag-NP/chitosan nanocomposites were effective against *E. coli* and *S. aureus*.

In 2023, da Silva et al. [57] investigated Ag-NPs sputtered onto a polylactic-acid biopolymer under fixed operating parameters (10 sccm argon flow, 0.2 A discharge current, 40 W discharge power, 200 kHz pulse frequency, 2 ms duty cycle, 2.7 Pa working pressure). The resulting coatings prevented biofilm formation by *E. coli* and *B. subtilis* and showed antiviral activity against the Omicron variant of SARS-CoV-2, underscoring the versatility of plasma-based Ag-NP coatings against both bacterial and viral pathogens.

5.4. Electron-Beam (E-Beam) Deposition

Electron-beam deposition produces densely packed layers of Ag-NPs [58]. In 2018, He et al. [59] generated a nanocomposite coating ($AgNO_3$(cr) and polylactic acid) from an active gas phase under vacuum (4×10^{-3} Pa), using an electron gun with a filamen-

tary cathode delivering low-energy beams (current density j = 0.01–0.03 A cm^{-2}, energy 1000–2000 eV). FTIR confirmed the interaction between the resulting Ag-NPs (average diameter 17.5 ± 1.13 nm) and the polymer matrix, and the coatings displayed excellent antibacterial activity against *E. coli* ATCC 25922 and *S. aureus* ATCC 12600. Gao et al. [60] instead used e-beam irradiation to reduce silver sulfadiazine into Ag-NPs supported on polyvinyl alcohol (PVA); the resulting hydrogels showed strong antibacterial activity against *E. coli* and *S. aureus* independent of the irradiation dose used (5–45 kGy).

Lampé et al. [61] deposited Ag-NPs (average size 58 nm) onto dental titanium implants using an Electron Cyclotron Resonance Ion Source (oxygen support gas, 1123–1223 K), obtaining coatings with significant activity against *S. aureus* ATCC 29213—a finding relevant to the prevention of peri-implantitis. Kim et al. [62] irradiated poly(vinylpyrrolidone)-stabilised silver nanowire films with a low-energy e-beam (up to 1200 kGy for 45 s) and reported that irradiation raised the log-reduction of bacterial counts from 1.2 to 1.4 for *S. aureus* and from 1.5 to 3.7 for *E. coli* after one hour of contact.

In 2023, Chiangnoon et al. [63] used e-beam irradiation to prepare Ag-NP-loaded PVA hydrogel dressings; diffusion assays showed minimal inhibitory concentrations of 0.25 and 0.5 mg cm^{-2} against *E. coli* and *S. aureus*, respectively—results that support their use in wound-care dressings.

5.5. Evaporation/Condensation (E/C)

Historically, metallic nanoparticles have been prepared by E/C in a temperature-controlled oven under inert atmosphere [64], including by inert-gas condensation (IGC) and co-condensation (CoCON). The IGC method can generate a substantial yield of metallic nanoparticles within only five minutes using a helium-fed plasma-jet flame [65], while extremely fine particles (<10 nm) have also been obtained under vacuum at an oil surface [66]. In CoCON, the metal is evaporated either at the surface of a running oil film under vacuum [67] or in the presence of a frozen organic solvent such as toluene [68].

In 2020, Park et al. [69] prepared ultra-small Ag-NPs under gas flow using E/C and evaluated their antibacterial activity and stability against *E. coli* and *Staphylococcus epidermidis* (*S. epidermidis*), reporting a practical route to continuously manufacture ultrasmall (~0.234 nm) particles active against a broad spectrum of bacteria. In 2022, Sakono et al. [70] developed a method for immobilising E/C-derived Ag-NPs onto a glass plate but did not report an antimicrobial application. In 2023, however, Vasil'kov et al. [71] prepared Ag-NPs by E/C in 2-propanol under high vacuum (10^{-4}–10^{-5} Torr), stabilised over a hyperbranched polyaminopropylalkoxysiloxane matrix; TEM revealed an average particle size of 5.3 nm, and the resulting material showed strong antimicrobial activity against *B. subtilis* and *E. coli*. The same group also prepared Ag-NPs supported on bacterial cellulose (mostly <3 nm, as shown by XPS and TEM) that were active against *B. subtilis*, *S. aureus* and *E. coli*.

5.6. Microwave Irradiation (MWI)

Seku et al. [72] used a microwave-assisted route to prepare Ag-NPs and examined their catalytic, antibacterial and antioxidant activities. Kumar et al. [73] deposited Ag-NPs on single-walled carbon nanotubes by MWI, finding that complete reduction of Ag^+ from $AgNO_3$ occurred within 40 s at 500 W; the resulting materials showed excellent antibacterial activity against *S. aureus* and *E. coli* and were used to impart durable antibacterial finishing to cotton fabric. Araruna et al. [74] used a green, MW-assisted route to prepare cashew-gum-stabilised Ag-NPs, finding that alkaline conditions gave more efficient conversion of $AgNO_3$ and well-dispersed, spherical, stable particles with promising activity, particularly against Gram-negative bacteria.

In 2023, Aljohani et al. [75] prepared chitosan-stabilised Ag-NPs entrapped within polyethylene oxide nanofibers by MWI; the materials showed strong antibacterial activity against *E. coli* and *S. aureus* (inhibition zones of 51.2 ± 3.2 mm and 47.2 ± 2.1 mm, respectively) while remaining innocuous toward human skin fibroblasts and keratinocytes (>93.5% viability), supporting their potential for wound-care applications. Using the same technique, Mpala et al. [76] prepared cellulose-nanocrystal-mediated Ag-NPs and reported good activity against *E. coli*, *P. aeruginosa*, *S. aureus*, *Staphylococcus epidermidis* and *Staphylococcus saprophyticus*, with a view toward biofouling control in membrane distillation.

Overall, physical methods remain a well-established, reproducible route to size- and shape-controlled Ag-NPs. Their principal drawback—the substantial energy demand of techniques such as LA and e-beam deposition—has sustained a persistent demand for less energy-intensive alternatives. A more direct comparison of the individual techniques, including their scalability and suitability for biomedical use, is given in Section 7.5.

6. Antibacterial Activity of Ag-NPs Obtained by Chemical Methods

The chemical synthesis of Ag-NPs requires a silver precursor, a reducing agent and a stabiliser. The stabiliser prevents nanoparticle agglomeration and plays a key role in controlling size and shape. As Ag^+ is reduced to Ag^0, colloidal Ag-NPs form via two sequential processes—nucleation and growth (Figure 3) [11]—of which nucleation requires high activation energy while growth proceeds at comparatively low energy [77]. The final size and shape of the Ag-NPs depend on the relative rates of these two processes, which can in turn be tuned via reactant concentration, reaction temperature, pH, and related parameters.

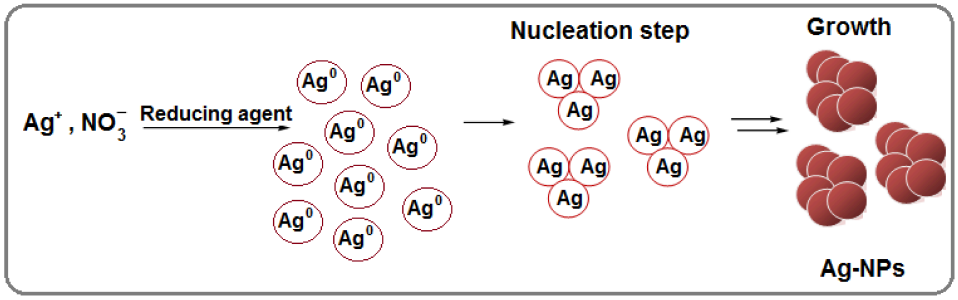


Figure 3. Mechanism of Ag-NP formation via chemical reduction of Ag^+, adapted from Burda et al. [11].

6.1. Basic Chemical Reduction Methods

The chemical synthesis of Ag-NPs was first reported by Lee and Meisel [78] and by Creighton et al. [79]. The former method used $AgNO_3$ and sodium citrate as the reducing agent to obtain Ag-NPs of varying size, whereas the latter reduced Ag^+ with sodium tetrahydroborate ($NaBH_4$) to yield particles with a narrow size distribution (~10 nm). Ag-NPs can also be prepared via the (modified) Tollens method [80], in which the diamminesilver(I) complex is reduced by organic agents such as aldehydes or sugars:

$$[Ag(NH_3)_2]^+(aq) + R\text{-}CHO(aq) \rightarrow Ag(cr) + RCOOH(aq) \quad (1)$$

According to Yin et al. [80], Ag-NP formation by this route proceeds through at least three distinct stages: (i) nucleation, (ii) growth and aggregation, and (iii) Ostwald ripening of the aggregates into discrete, uniformly sized particles, as confirmed by TEM.

Recent work on the chemical reduction of Ag^+ (from $AgNO_3$ solution) and the resulting antimicrobial activity is summarized in Table 4.

Table 4. Ag-NPs prepared from $AgNO_3$ by chemical reduction: antimicrobial activity.

Reducing Agent	Stabiliser	Bacterial Target	Size/Shape	Reference
$NaBH_4$	Ethanol	*B. subtilis*, *P. aeruginosa*	18.31 nm, spherical	[81]
Sodium citrate	-	*E. coli* ATCC 25922, *S. aureus* ATCC 33591	14.47 nm, rectangular/spherical	[82]
$NaBH_4$	Sodium citrate	*E. coli*, *Enterococcus faecalis*	3.14 ± 0.54 nm, spherical	[83]
$NaBH_4$	PEGMA (a)/polyacrylic acid	*S. aureus*, *E. coli*	4 ± 1.5 nm, spherical	[84]
Ethylene glycol/tetraethyleneglycol pyrrolidone	PVP	*E. coli*, *S. aureus*	15.58–72.44 nm, spheres/rods	[85]
Starch (boiled rice water)	PVA/montmorillonite film	*Salmonella Typhimurium*, *S. aureus*	n.d.	[86]
Starch	Chitosan	*P. aeruginosa*, *E. coli*, *K. pneumoniae*, *S. Typhimurium*	~20 nm, spherical	[87]
Glucose, sucrose, dextran	-	*E. coli*, *S. aureus*	15–30 nm	[88]
DMF	-	*S. aureus*, *E. coli*	2.18–7.39 nm, spherical	[89]
DMF	Silicon derivative (b)	*S. mutans*, *S. sobrinus*	n.d., spherical	[90]
Hydrazine hydrate	Benzyl alkyl ionic liquids	*S. aureus*, *K. pneumoniae*, *P. aeruginosa*, *E. faecium*, *A. baumannii*, *Enterobacter* spp.	1.5–2.9 nm	[91]
Formaldehyde	-	*E. coli*, *S. aureus*	10–100 nm, spherical	[92]
Sodium tartrate/citrate	-	*E. coli*, *K. pneumoniae*, *S. Typhimurium*, *P. aeruginosa*, *S. aureus*	125.4 nm (DLS), spherical	[93]
Cyclodextrin	-	*P. aeruginosa*	5–20 nm (DLS), near-spherical	[94]
$NaBH_4$	PVA/PVP (c)	*S. aureus*, *E. coli*	15 nm, spherical	[95]
Sodium citrate	Glycerol and PVP	*multiple* ATCC strains	31.2 nm, spherical	[96]
Pectin	-	*B. pumilus*, *B. subtilis*, *E. coli*	8–28 nm, spherical	[97]
Glucose	PVA	*S. aureus*, *E. coli*	15–25 nm, semi-spherical	[98]
Ascorbic acid/thymol/usnic acid	-	*MRSA*, *A. baumannii*, *K. pneumoniae*	21.7–94.2 nm, spherical and rods	[99]
Gallic acid	Chitosan	*E. coli* ATCC 10536	26.23 ± 9.92 nm, spherical	[100]

Table 4. *Cont.*

Reducing Agent	Stabiliser	Bacterial Target	Size/Shape	Reference
Tannic acid	-	*E. coli*, *K. pneumoniae*, *A. baumannii*, *P. aeruginosa*, *S. aureus*.	16.82 nm, cubic	[101]
Tannic acid	Sodium alginate	*S. aureus*	18.52 ± 0.07 nm, spherical	[102]
$NaBH_4$	Phosphonium surfactant	*S. aureus*, *E. coli*	40–109 nm	[103]
Sodium hypophosphite/hydroxylamine hydrochloride/gallic acid + caffeine/$NaBH_4$ + amino acids	SHMP (d)	*E. coli*, *S. aureus*	10–15 nm, spherical	[104]

(a) Poly(ethyleneglycol)methylether methacrylate. (b) 3-aminopropyltrimethoxysilane. (c) Polyvinyl alcohol/polyvinylpyrrolidone. (d) Sodium hexametaphosphate.

According to Table 4, most reducing agents and stabilisers favour spherical Ag-NPs. Notably, however, Ag nanocubes (mean edge length 55 ± 5 nm) were obtained by Yu and Yam [105,106] by reducing the diamminesilver(I) complex with glucose at 393 K in the presence of n-hexadecyltrimethylammonium bromide (HTAB). In another study, Zielinska et al. [107] prepared silver nanowires in two steps: first, spherical Ag-NPs (4 nm) were obtained from $AgNO_3$ using $NaBH_4$ and sodium citrate as reducing and stabilising agents, respectively; a subsequent treatment of these nanospheres with $AgNO_3$ and ascorbic acid then yielded silver nanorods and nanocables.

Specific polymers can also be added to the synthesis medium to obtain Ag-NPs of a particular shape. For instance, mixing $AgNO_3$ and ethylene glycol in the presence of polyvinylpyrrolidone (PVP) as a stabiliser gives nanospheres, nanocubes, nanobars or silver nanowires (Figure 4); in general, the concentration of the stabilising polymer is the parameter that most strongly determines the final size and shape of the Ag-NPs [108].

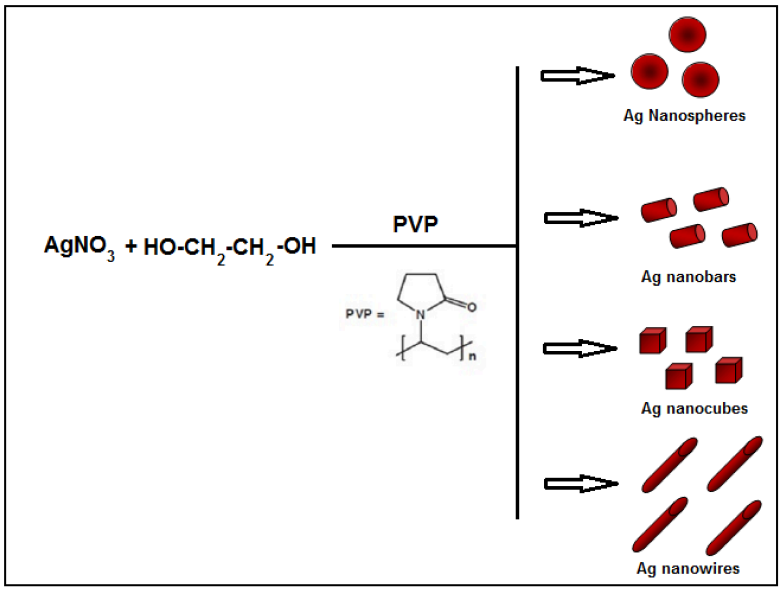


Figure 4. Silver nanostructures obtained by reducing silver nitrate in ethylene glycol using polyvinylpyrrolidone as a stabilising agent, adapted from [24,108].

Table 4 also shows that, despite their generally successful outcomes, several of these procedures rely on hazardous chemicals such as DMF, $NaBH_4$, hydrazine and formaldehyde (see, respectively, the corresponding Sigma-Aldrich safety data sheets, SDS N° 227056, 452882, 225819 and F8775). This has motivated the development of alternative routes designed to minimise the use of toxic reagents.

6.2. Electrochemical Methods

Electrochemical synthesis of Ag-NPs offers several advantages, including a simple single-vessel setup, easy control of the reaction conditions, and the use of comparatively benign reactants. Yan et al. [109] applied a cathodic voltage of 5 V to deposit Ag-NPs on a chitosan multilayer hydrogel film, obtaining spherical particles (~15 nm average size) that conferred substantial antibacterial activity to the hydrogel, as evaluated by disc diffusion (90 mm plates, Luria–Bertani agar) against *S. aureus* and *E. coli* (10^5–10^6 CFU mL^{-1}).

Zhang et al. [110] combined a triboelectric nanogenerator with a capacitor to electrodeposit sub-10-nm Ag-NPs, achieving overwhelming antibacterial efficiency against *E. coli* and *S. aureus* (100% efficiency within 2 h) and demonstrating clear superiority over conventional direct-current deposition. More recently, Sudhisha et al. [111] studied Ag-NP-doped poly(3,4-ethylenedioxythiophene) (PEDOT) deposited on anodised TiO_2 nanotubes for orthopaedic applications; the Ag-NP/PEDOT coating displayed excellent antibacterial activity against both Gram-positive and Gram-negative bacteria.

6.3. Sonochemical Methods

The sonochemical synthesis of metallic nanoparticles relies on acoustic cavitation: micrometre-sized gas bubbles collapse and implode within the medium (typically water), generating highly reactive free radicals that reduce noble-metal ions [112]. Andrade Neto et al. [113] used this approach (20 kHz ultrasonic tip) to prepare semi-spherical Ag-PbS nanoparticles that showed interesting antimicrobial activity, evaluated by agar diffusion, against *E. coli* ATCC 25922, *S. aureus* ATCC 25923. Sorinezami and Ghanbari [114] prepared chitosan-supported Ag-NPs (~30 nm) by mixing $AgNO_3$ and $NaBH_4$ in deionised water under ultrasonic irradiation (150 W, 30 min); the resulting nanocomposites showed marked activity against *E. coli*.

Tzounis et al. [115] reported a versatile route to manufacture low-cost antimicrobial surgical equipment: a surgical retractor 3D-printed from polylactic acid was coated with Ag-NPs (from $AgNO_3$, ethylene glycol and PVP; average size 31.08 ± 6.68 nm) by sonochemical deposition, yielding vigorous antimicrobial activity against *S. aureus*, *P. aeruginosa* and *E. coli*. Shepida et al. [116] combined sonochemical and electrochemical routes (cyclic voltammetry, −1.0 to +1.0 V, in a rhamnolipid biosurfactant solution under 22 kHz ultrasound) to obtain very small Ag-NPs (1–3 nm), and found that increasing the rhamnolipid concentration from 1 to 4 g L^{-1} raised both the anodic/cathodic current and the rate of Ag-NP formation; the resulting particles were active against *E. coli* and *S. aureus*. Zozulya et al. [117] likewise combined galvanic replacement of Ag^+ on aluminium powder with ultrasonic irradiation (20 W, 20 kHz) in sodium polyacrylate solution, obtaining ~25 nm Ag-NPs with good activity against Gram-negative and Gram-positive bacteria as well as fungi.

In 2023, Abazari et al. [118] prepared Ag-NP-coated spunbond fabrics using a high-intensity probe sonicator (20 kHz, 400 W, 60% efficiency) in a water/ethanol/ethylene-glycol solution of $AgNO_3$ under argon, followed by ammonia treatment. Longer sonication times and higher precursor concentrations gave larger, more stable coatings with lower silver release. The coated fabrics were active against *E. coli* and *S. aureus*, showed no significant cytotoxicity toward HEK293 cells or *Artemia* nauplii, and were proposed as candidates for reusable facemasks.

6.4. Photoreduction

The main advantage of photoreduction is that it avoids hazardous chemical reducing agents entirely. In 2018, Courrol et al. [119] prepared Ag-NPs by femtosecond-laser photoreduction of $AgNO_3$ in a tryptophan solution and evaluated their activity against *E. coli*, finding that both nanoparticle concentration and laser energy strongly influenced bactericidal efficacy—irradiation at ~300 µJ for 60 min gave the highest activity, attributed to kynurenine, a tryptophan photolysis product. Van Viet et al. [120] used a green, low-power-UV photoreduction route in the presence of PVP, optimising the ethanol:water ratio, the $AgNO_3$:PVP ratio, pH and reaction time; the resulting spherical Ag-NPs (average size 16 ± 2 nm, 35 ppm) achieved close to 100% elimination of *E. coli*. The same group [121] later loaded Ag-NPs onto TiO_2 nanotubes by UVC photoreduction (18 W, 254 nm, 24 h, room temperature, no additional reducing agent), obtaining uniformly distributed 5 nm particles that eliminated 99.99% of *S. aureus* within 60 min under sunlight irradiation (20 ppm).

Paiva et al. [122] performed a one-step photoreduction of Ag-NPs within a glass-ionomer cement (GIC) for dental applications, obtaining small, dispersed spherical particles (~6 nm); at 0.50 wt% Ag, activity against *E. coli* (Ag^+ diffusion assay) and *S. mutans* (MTT assay) increased significantly with silver content. In 2020, Villanueva et al. [123] embedded photoreduced Ag-NPs within highly functionalised oligomers (from ethylene glycol diglycidyl ether, imidazole and methacrylic acid), which promoted strong adhesion of the particles to a polystyrene substrate and improved activity against both Gram-positive and Gram-negative bacteria.

In 2023, Dong et al. [124] prepared Ag-NP-loaded polyvinylidene fluoride (PVDF) ultrafiltration membranes by in situ UV photoreduction, achieving ~99% inhibition of *E. coli* after 24 h. Poudel and Kim [125] prepared Ag-NP-decorated TiO_2 nanoflakes (2 wt% Ag) by a solvothermal-photoreduction sequence and reported markedly higher antibacterial activity against *S. aureus* and *E. coli* compared with bare TiO_2 nanoflakes.

In summary, chemical synthesis routes for Ag-NPs are efficient and versatile but carry a real disadvantage in that many rely on hazardous chemicals or ionising radiation. This has driven a marked shift in the field toward biological methods, which are generally faster, cheaper and more environmentally sustainable.

7. Antibacterial Activity of Ag-NPs Obtained from Plant Extracts

There is a sustained demand for synthetic routes to Ag-NPs that are economical, commercially viable and environmentally friendly. Biological synthesis meets these criteria particularly well, since it requires neither high pressure nor high temperature, nor the use of toxic chemicals [126,127]. Biosynthesis of Ag-NPs was first reported in 1984 using *Pseudomonas stutzeri* AG259 [128] under ambient conditions, a method that already allowed some control over particle size and shape.

Using plant extracts as reducing and stabilising agents offers good control over crystal nucleation and growth [129]. Virtually any part of the plant—leaf, root, stem, fruit, seed, gum, rhizome, etc.—has been used for Ag-NP synthesis [10,130].

Typically, the chosen plant material is first washed with tap water and then with distilled water to remove unwanted debris, dried and ground into a powder (or used fresh), and extracted by heating in deionised water or alcohol below 60 °C for a few hours. The resulting extract is then added to a silver-salt solution and heated at a chosen temperature [10]. Nanoparticle formation can be monitored visually (colour change) or by UV-Vis spectroscopy; at the end of the reaction, the Ag-NPs are recovered by centrifugation, washed and dried at low temperature [10].

Plant extracts typically contain alkaloids, proteins, enzymes, amino acids, alcohols and polysaccharides, which drive the reduction of silver ions to Ag-NPs [131]; some extracts

additionally contain quinones and chlorophyll pigments that contribute both to reduction and to nanoparticle stabilisation [132].

7.1. Chemistry of Ag^+ Reduction and Nanoparticle Stabilisation

In plant-mediated synthesis, the extract plays three roles at once: it supplies the electrons that reduce Ag^+ to Ag^0, it provides nucleation sites and then limits growth, and it coats the finished particle. The reducing power comes mainly from phenolic compounds. The hydroxyl groups of polyphenols such as gallic, ellagic and chlorogenic acid, and of flavonoids such as quercetin and the catechins, can be oxidised to quinones while transferring electrons to Ag^+, after which Ag^0 atoms nucleate and grow as described for chemical reduction in Section 6 [127,130]. Flavonoids are also proposed to reduce silver through keto-enol tautomerisation, the enol form releasing a reactive hydrogen atom, and those with free hydroxyl and carbonyl groups can chelate Ag^+ before reduction, which probably favours the formation of small, uniform nuclei [127,133]. Terpenoids are thought to act in a similar way through their hydroxyl and aldehyde groups, although the evidence is more circumstantial, since most studies simply detect them by FTIR before and after the reaction.

Reducing sugars (through their aldehyde groups, comparable to the Tollens-type reaction in Equation (1)), ascorbic acid and some organic acids contribute in a similar manner. Proteins and enzymes take part in two ways. Electron transfer to Ag^+ by enzymes and by amino acid residues with reducing side chains (tyrosine, tryptophan, cysteine) has been proposed, although this is better documented for microbial systems. More important for the product, proteins bind to the particle surface through amine, carboxylate and thiol groups and prevent aggregation, while polysaccharides and pectins act mainly as steric and electrostatic stabilisers. Amide and hydroxyl bands in the FTIR spectra of purified particles are the usual evidence for such capping, but they show that organic matter is present at the surface, not which compound reduced the silver [127,130].

Two points follow from this chemistry. First, the molecules that reduce Ag^+ stay on the surface, so a "green" particle never has a bare metal surface, and its coating changes with the extract; this affects surface charge, ion release and biological interactions (Sections Linking Physicochemical Properties to Antimicrobial Performance and 8). Second, polyphenols are consumed in the redox step while other constituents merely adsorb, so any change in the polyphenol:Ag^+ ratio, pH or temperature alters the balance between nucleation and growth and hence the size distribution. This helps to explain the broader size distributions that we mentioned in the Introduction: a mixture of reductants with different potentials and rates lets nucleation continue for longer than a single fast reductant such as $NaBH_4$ does.

7.2. Influence of Extract Composition and Reaction Conditions

Differences between extracts translate into differences in the particles. Table 5 gives a rough idea: *Selaginella bryopteris* yielded 5–10 nm monodisperse spheres [134], extracts of *Salvia spinosa* gave particles spanning 19–125 nm [135], and the mixture of date palm, asafoetida and acacia extracts gave particles of 68 and 156 nm [136]. An extract rich in low-molecular-weight phenolics tends to promote fast nucleation and small particles, whereas extracts with a high content of proteins and polysaccharides, or of high-molecular-weight tannins, tend to give larger or more polydisperse particles, because stabilisation is slow or particles are bridged [127,133]. Part of this variation belongs to the plant itself and part to the way the extract was made: plant organ, season and place of harvest, solvent and extraction temperature all change the phytochemical profile [13].

Reaction conditions act on top of this. Higher pH deprotonates phenolic hydroxyl groups and usually accelerates reduction, giving smaller particles, whereas low pH favours aggregation; a higher temperature speeds up nucleation; and the Ag^+:extract ratio and

the $AgNO_3$ concentration (most studies work at millimolar levels) decide whether nucleation or growth dominates. Statistical designs such as the Box–Behnken approach used for pomegranate peel by Díaz-Puertas et al. [137] are a useful way of mapping these interactions, because they allow the effects of $AgNO_3$ concentration, extract concentration and temperature on hydrodynamic size, polydispersity and zeta potential to be examined together instead of one variable at a time.

Extract composition also affects antimicrobial performance, indirectly through size, shape and surface charge (Section Linking Physicochemical Properties to Antimicrobial Performance) and directly because residual phenolics, some of which are antimicrobial in their own right, may add to or interfere with the action of silver. In the work of Khorrami et al. [138] on black-peel pomegranate, for instance, the extract alone was bacteriostatic whereas the particles were bactericidal, and the two effects are hard to separate. Controls with the extract alone, and with Ag^+ at an equivalent silver content, should be included routinely; they are not reported in all of the studies we reviewed.

Table 5. Selected plant extracts used for the green synthesis of Ag-NPs and their antimicrobial activity.

Plant Source	Size/Shape	Bacterial Target	Reference
Phoenix dactylifera, *Ferula asafetida*, *Acacia nilotica*	67.8 ± 0.3 and 155.7 ± 1.5 nm, spherical	*S. aureus*, *P. aeruginosa*, *E. coli*	[136]
Garlic extract, alone or with ginger	20–70 nm, spherical	*S. aureus*, *E. coli*	[139]
Selaginella bryopteris	5–10 nm, spherical/monodisperse	*E. coli* (NCIM-5051), *S. aureus*	[134]
Salvia spinosa	19–125 nm	*B. subtilis*, *B. vallismortis*, *E. coli*	[135]
Azadirachta indica, *Syzygium cumini*	10–20 nm (*A. indica*), 25–30 nm (*S. cumini*), spherical	*B. subtilis*, *E. coli*	[140]
Bergenia ligulata, *Rheum australe*, *Selinum vaginatum*	5–15, 20–50, 10–30 nm respectively	*Salmonella Typhi*, *B. cereus*, *P. aeruginosa*	[141]

7.3. Representative Examples, Including Plant-Waste Extracts

Because the entries in Table 5 say little about agro-food waste, which is the part of the field with the clearest sustainability argument, Table 6 collects more recent examples based on peels and other by-products. It reports synthesis conditions, characterisation methods and cytotoxicity data where the original papers provide them. Yield is not tabulated because only a minority of studies measure it, and those that do express it as Ag^+ conversion or as mass of dry particles, in different units, so that no meaningful comparison is possible. We regard the absence of yield and mass-balance data as a gap in the field, since claims of scalability depend on them.

Two observations stand out. First, the peel studies agree on spherical particles in the low tens of nanometres (19 and 23 nm in the two studies that report size), with potency expressed as MIC values between about 30 and 250 µg/mL where these are given. Second, and more important for biomedical use, Mafhala et al. [143] found an IC_{50} of about 38 µg/mL on HEK293 cells, which is of the same order as the MIC against the Gram-positive strains (31.25 µg/mL) and well below the MIC against the Gram-negative ones (250 µg/mL). Given the different assays and exposure times, the comparison is approximate, but it suggests that the concentrations needed to act on *E. coli* would be toxic to the human cell line, and that those acting on *S. aureus* leave almost no margin. A green origin does not by itself guarantee

a favourable therapeutic window, and the same comparison should be made for every new formulation (Section 8).

Table 6. Plant-waste (peel) extracts used for the green synthesis of Ag-NPs: synthesis conditions, characterisation, antimicrobial activity and cytotoxicity.

Plant Source	Synthesis Conditions	Characterisation	Size/Shape/ Zeta Potential	Antimicrobial Activity	Cytotoxicity	Ref.
Pomegranate (*Punica granatum*) peel waste	Peel extract (phenol the main GC-MS constituent, 51.1%) reacted with a silver salt; yellow-to-brown colour change	UV-Vis (SPR at 440 nm), SEM, FTIR, zeta potential	Spherical (SEM); zeta potential −20.1 mV	Active against all eight foodborne strains tested (six bacteria, two moulds); strongest on *B. subtilis*, then *K. pneumoniae*; weakest on *R. oryzae*	n.r.	[142]
Naartjie (*Citrus unshiu*) fruit peel	20 mL aqueous peel extract added to 0.5 g $AgNO_3$; immediate colour change	UV-Vis (SPR at 424 nm), SEM, TEM, XRD, FTIR	Spherical, mean 23 nm; crystalline	MIC 31.25 µg/mL for *S. aureus* and *B. cereus*; 250 µg/mL for *E. coli* and *S.* Typhimurium	MTT: IC_{50} 37.73 ± 0.34 µg/mL (HEK293); 56.37 ± 0.73 µg/mL (A549)	[143]
Orange (*Citrus sinensis*) peel	Aqueous peel extract (polyphenol-rich agro-industrial by-product) as reducing agent	UV-Vis, DLS, SEM, EDX, TEM	n.r.	MIC 32 µg/mL for both *E. coli* and *S. aureus*; also tested on *C. albicans* and on biofilm formation	n.r.	[144]
Black-peel pomegranate (*P. granatum*) peel	Aqueous peel extract	n.r.	Spherical, mean 19 nm; zeta potential −33 mV	MBC 40–65 µg/mL; extract alone bacteriostatic (no MBC)	n.r.	[138]
Pomegranate (*P. granatum*, "Mollar de Elche") peel	$AgNO_3$ concentration, extract concentration and temperature optimised by a Box–Behnken design	DLS (hydrodynamic diameter, polydispersity), zeta potential	Optimised responses; values depend on the design point	Substantial activity against *E. coli* and *S. aureus*; partly retained after incorporation into nanofibrous scaffolds	n.r.	[137]

n.r., not reported. SPR, surface plasmon resonance; MTT, tetrazolium-based viability assay.

7.4. Recent Trends in the Literature (2024–2026)

Green, plant-mediated synthesis continued to dominate the literature published between 2024 and 2026. Eker et al. [13] reviewed how the phytochemical composition of the extract used—and not only the plant species itself—governs the morphology, stability and multifunctional bioactivity of the resulting Ag-NPs. In a systematic review restricted to *Klebsiella* spp. and covering studies published between 2015 and 2025, Dunah et al. [14] confirmed that plant-mediated Ag-NPs remain consistently effective, including against multidrug-resistant clinical isolates.

A second trend is that antimicrobial resistance (AMR) is now discussed as a central issue rather than a side note. Khalifa et al. [15] reviewed Ag-NPs as "next-generation" antimicrobial agents against multidrug-resistant bacteria, but also stressed the persistent challenges—cytotoxicity, environmental persistence and the possibility that Ag-NPs themselves could select for bacterial silver resistance. Jangid et al. [16] reached a similar conclusion for food-safety applications: biogenic Ag-NPs are active against foodborne pathogens such as *E. coli*, *Salmonella enterica* and *Listeria monocytogenes*, yet silver bioaccumulation, environmental toxicity and unclear regulatory status still limit their large-scale use.

Physical methods have not been abandoned either. In 2025, Hamid et al. [26] showed that the energy of the laser used in laser ablation can be adjusted to tune both the size and the antibacterial potency of the resulting Ag-NPs, which confirms that reagent-free

physical routes still have something to offer alongside green synthesis. At the same time, an updated toxicological synthesis [17] called for more standardised characterisation and dose-reporting across the field—a gap that becomes obvious as soon as one tries to compare, for example, the entries of Tables 4 and 5 of this review.

7.5. Comparison of Physical, Chemical and Plant-Mediated Routes

To put the three families of methods on a common footing, Table 7 summarises how the individual techniques covered in Sections 5–7 compare on the criteria that matter for application. The ratings are qualitative and reflect the studies cited in this review; head-to-head experiments between routes hardly exist.

Table 7. Qualitative comparison of the synthesis routes discussed in this review.

Method	Control of Size and Shape	Scalability	Energy and Environmental Burden	Main Limitations	Best-Suited Use
Laser ablation in liquid	Good; tuned by fluence, wavelength, pulse length and medium, but distributions can be bimodal [41]	Low to moderate	High energy; no reagents	Low productivity; equipment cost; re-irradiation needed to narrow size	Ligand-free colloids for small-volume, research-grade work [43,44]
CVD/ALD	Excellent control of film thickness; particles grown as islands on a substrate	Moderate for coatings; not applicable to colloids	High (vacuum, 363–423 K, volatile fluorinated precursors)	Costly precursors; coatings only	Conformal coatings on implants, filters and masks [51,53,54]
Plasma-assisted	Moderate to good; exposure time and precursor concentration	Moderate; plasma jets and sputtering already used industrially for coatings	Moderate; no reducing agent	Reproducibility between reactors; little stability data	Coatings on polymers and biopolymers [56,57]
Electron beam	Moderate; dose-dependent	Low to moderate	High (accelerator, vacuum for deposition)	Specialised facilities; ionising radiation	Hydrogel dressings and polymer coatings [60,63]
Evaporation/condensation	Good for very small particles	Moderate	High (vacuum, heating)	Few antimicrobial studies; handling of dry powders	Ultrafine particles and supported composites [69,71]
Microwave irradiation	Good; fast and uniform heating	Moderate; limited by cavity size	Low to moderate (short reaction times)	Often combined with chemical reductants or stabilisers	Rapid preparation of stabilised colloids and composites [73–76]
Chemical reduction (citrate, $NaBH_4$, polyols)	Very good; reductant, stabiliser, temperature and pH; cubes, rods and wires accessible	High	Low energy; hazardous reagents ($NaBH_4$, hydrazine, DMF)	Reagent residues; toxic capping agents [103]; aggregation	Applications in which residues can be fully removed; industrial scale
Electrochemical, sonochemical, photoreduction	Good to very good	Moderate; limited by cell volume, cavitation or light penetration	Low to moderate	Mostly laboratory scale; additives still common	Functionalisation of membranes, textiles and implants [110,115,124]
Plant-mediated	Moderate to poor; broad distributions that depend on the extract	Potentially high (mild, aqueous), but extract varies between batches	Low; waste valorisation possible	Variable extract composition; reproducibility; unknown capping layer; incomplete mechanistic understanding	Uses that tolerate polydispersity (food packaging, water treatment, topical products); biomedical use only with strict characterisation

Three conclusions can be drawn from Table 7. For control over particle size and morphology, chemical reduction in solution is the most versatile route: reductant, stabiliser, temperature and pH can all be varied, and it is the only route in this review that has

produced cubes, rods and wires on demand (Section 6.1). Laser ablation and evaporation/condensation give the cleanest surfaces but fewer handles on shape. For scalability, solution chemistry and plant-mediated synthesis are the easiest to scale in volume, while vacuum- and beam-based techniques scale only as coating processes and at high capital cost. Plant-mediated synthesis is usually described as scalable, but the studies discussed here are almost all laboratory-scale, and reproducibility across extract batches is seldom reported. For biomedical use, where purity, reproducibility and a well-defined surface are the priorities, physical routes that give ligand-free particles, and chemical routes in which reagents can be completely removed, are at present arguably the safer choice for colloids, whereas the physical deposition methods are best suited to coatings on implants and devices. Plant-mediated particles are attractive where some polydispersity is acceptable and where cost and environmental load matter more, as in food packaging, water treatment and topical products. They will need much better standardisation of the extract before they can be considered for parenteral or implantable use. Figure 5 places the elements discussed so far (route, properties, characterisation, mechanism and outcome) in a single scheme.

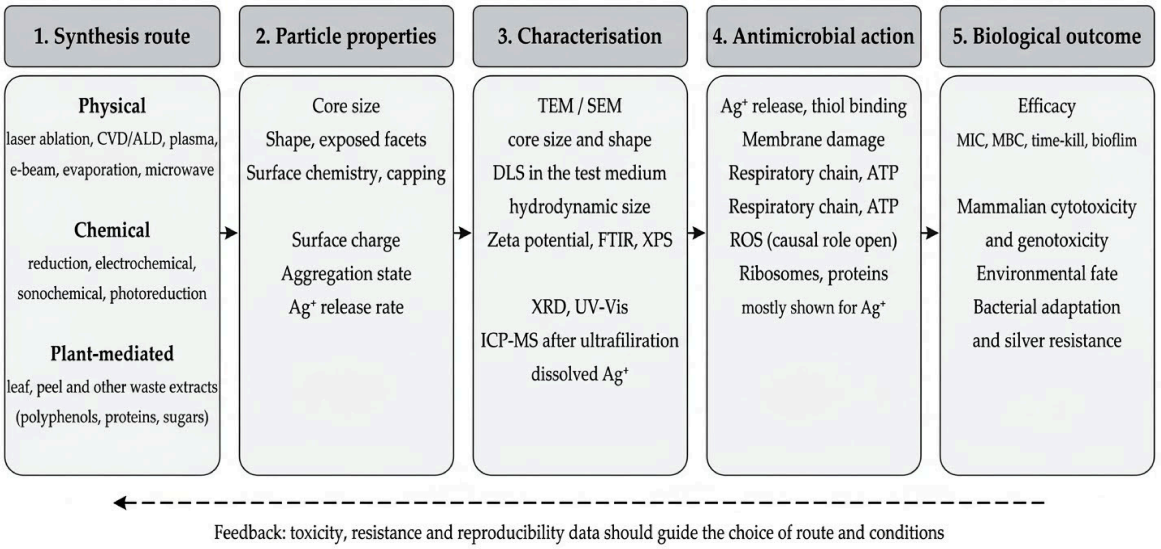


Figure 5. Conceptual overview linking the synthesis route, the physicochemical properties of Ag-NPs, their characterisation, the proposed antimicrobial mechanisms and the biological outcome, including toxicity and resistance.

8. Toxicity, Environmental Fate and Long-Term Safety

What makes Ag-NPs useful against bacteria, namely their reactivity towards thiols and the release of Ag^+, also acts on mammalian cells and on other organisms, and the selectivity is narrower than often assumed. This section brings together the main toxicological findings, with emphasis on the points that matter for the biomedical and food-related applications discussed above.

8.1. Cytotoxicity, Oxidative Stress and Genotoxicity in Eukaryotic Cells

In cultured human cells, Ag-NPs enter mainly by endocytosis and are then partly dissolved in the acidic endolysosomal compartment, releasing Ag^+ inside the cell, an effect sometimes described as a "Trojan horse" mechanism. In human lung fibroblasts and glioblastoma cells, AshaRani et al. [145] showed that Ag-NPs of roughly 6–20 nm impaired mitochondrial function, lowered ATP content, increased ROS and caused DNA damage and chromosomal aberrations in a dose-dependent manner. In human hepatoma (HepG2) cells, Kim et al. [146] linked toxicity to oxidative stress and to depletion of glutathione. The

oxidative-stress route is therefore the same one proposed for bacteria (Section 4.1), and it is hardly surprising that the concentration ranges overlap. Reported cytotoxic concentrations depend strongly on cell type, particle size, coating and exposure time, which makes it impossible to define a single "safe" dose [147].

DNA strand breaks, chromosomal aberrations and cell-cycle arrest have been described in cell models [145], generally at concentrations at which other signs of cytotoxicity are also present. Whether Ag-NPs are genotoxic at sub-cytotoxic doses, and in vivo, is less clear, and standard genotoxicity assays such as the comet and micronucleus tests are rarely included in antimicrobial studies. Some of the work reviewed above did include viability tests. The chitosan-stabilised Ag-NPs in polyethylene oxide nanofibres [75] kept more than 93.5% viability of fibroblasts and keratinocytes, and the coated fabrics of Abazari et al. [118] showed no significant toxicity towards HEK293 cells or *Artemia* nauplii. These results are encouraging, but they were obtained at the low silver release of the finished material, which is not the same as the toxicity of the free particles, and exposure times were short.

8.2. Biodistribution and Long-Term Exposure

Section 2 described the fate of ingested silver. Particles that are not dissolved in the stomach can reach the bloodstream and distribute to organs such as the liver and spleen before excretion [20]. Silver can also accumulate in tissue after chronic exposure: argyria following long-term use of silver compounds, including silver-containing wound dressings, is well documented [2]. For Ag-NPs, long-term low-dose data in humans are scarce and mostly come from animal studies or from exposure through dressings and consumer products. This is the gap we refer to in the Conclusions: efficacy data are produced much faster than information on what happens after months or years of exposure.

8.3. Environmental Fate and Ecotoxicity

Ag-NPs released from textiles, coatings and wastewater do not remain pristine. They are oxidised and, in sewage and anoxic sediments, largely converted to Ag_2S, which is far less soluble and much less toxic than the original particles, whereas in oxic freshwater chlorination and binding to organic matter modify them in other ways [28]. Sulfidation therefore reduces acute toxicity, but it concentrates silver in sewage sludge, which may be applied to agricultural land, and the long-term fate of this reservoir is uncertain. Because ionic silver is highly toxic to aquatic organisms even at low concentrations [28,147], ecotoxicity values obtained with pristine particles in clean water can over- or underestimate risk depending on the scenario. Ecotoxicological end points remain uncommon in the green-synthesis studies we reviewed.

8.4. Therapeutic Window and Implications for Green Synthesis

The key quantity for any biomedical use is the ratio between the concentration that harms host cells and the concentration that kills the pathogen. Few of the studies in Tables 3–6 report both. The data of Mafhala et al. [143] discussed in Section 7.3 show how narrow the margin can be even for a product made from plant waste. It is sometimes assumed that capping by phytochemicals makes green particles less toxic than chemically made ones, but the evidence is mixed. Phytochemical coatings may lower toxicity, in part by slowing dissolution; they may also contain bioactive compounds, vary between batches, and have rarely been compared with chemically synthesised particles of identical size and charge in the same cell model. Chemical protocols have their own problems, for example residual $NaBH_4$ or the cytotoxic surfactants mentioned in Section 6, and some physical routes give ligand-free particles whose surface is more reactive.

A fair summary is that no synthesis route has so far been shown to be intrinsically safe, and that safety has to be demonstrated for each product: particle characterisation, Ag^+ release, a mammalian cell panel with relevant cell types and exposure times, and, where possible, in vivo data. Reporting antibacterial and cytotoxicity end points on the same material, as done in refs. [75,118,143], is a practice we would encourage. The risk of selecting for silver resistance (Section 4.2) belongs in the same assessment, because a material that is safe for the patient but promotes resistance would still be a poor antimicrobial.

9. Conclusions

Antibacterial Ag-NPs can be obtained using the physical, chemical, and biological pathways covered in this review, but each has a drawback. Physical techniques, such as laser ablation, CVD/ALD, plasma, e-beam, evaporation/condensation, and microwave irradiation, give good control over particle size and, for some techniques, over shape, and do not leave chemical residues behind, but they are still energy-intensive and typically require expensive, specialised equipment, which restricts their use on a large scale.

Chemical reduction remains the most widely used method and the easiest to scale up, and it offers the widest range of particle shapes. However, a significant proportion of the documented protocols still depend on toxic reagents such as $NaBH_4$, hydrazine, DMF or formaldehyde, and residues of these substances, as well as of some stabilisers, are a real concern for biomedical and food-contact uses. Biological synthesis with plant extracts avoids most of these reagents, works under mild aqueous conditions and can valorise agro-food waste, and it attracted the largest number of new publications between 2024 and 2026. We regard it as a promising alternative rather than a universally superior strategy. Its limits are substantial: extract composition varies with species, organ, harvest and extraction method; reproducibility between batches is rarely documented; particle-size distributions are usually broader than in chemical or physical routes; the compounds responsible for reduction and capping are seldom identified; and scale-up of plant-based processes has hardly been demonstrated. Our comparison (Table 7) suggests that the best route depends on the intended use rather than on a general ranking.

Several aspects, in our view, warrant further consideration in the next endeavours. It is genuinely challenging to compare results because antibacterial activity is still reported using different protocols from one study to the next—disc diffusion, MIC, log-reduction—often without full particle-size distribution, surface charge, or precise inoculum density.

Three questions deserve priority in future work. First, the contributions of dissolved Ag^+ and of intact particles to the mechanisms outlined in Section 4 are still unresolved, and studies should report dissolved silver alongside the biological read-out. Second, the possibility that sub-lethal exposure selects for bacterial silver resistance, already demonstrated in the laboratory for ionic and nanoparticulate silver (Section 4.2), should be examined as a primary question rather than treated as a secondary issue as Ag-NPs get closer to clinical and food-safety uses. Third, new synthesis routes are being reported faster than toxicological evidence on long-term, low-dose exposure in humans and in the environment (Section 8). The few studies that measure antibacterial activity and cytotoxicity on the same material suggest that the therapeutic window can be narrow, even for products made from plant waste.

Overall, plant and plant-waste extracts are a promising basis for the next generation of antimicrobial Ag-NPs, provided that extract composition and synthesis conditions are standardised, particles are characterised in the medium in which they act, and toxicity and resistance data are produced together with efficacy data rather than afterwards. Whether silver nanoparticles can become a widespread complement to, or substitute for, conventional

antibiotics will depend on striking that balance between antibacterial efficacy, biocompatibility and environmental impact for each application.

Author Contributions: Conceptualization, A.M. and F.A.; writing—original draft preparation, A.M. and M.M.; writing—review and editing, A.M. and F.A. All authors have read and agreed to the published version of the manuscript.

Funding: This research received no external funding.

Institutional Review Board Statement: Not applicable.

Informed Consent Statement: Not applicable.

Data Availability Statement: No new data were created or analyzed in this study. Data sharing is not applicable to this article.

Conflicts of Interest: The authors declare no conflicts of interest.

References

1. Agency for Toxic Substances and Disease Registry (ATSDR). *Toxicological Profile for Silver*; U.S. Department of Health and Human Services, Public Health Service: Atlanta, GA, USA, 1990.
2. Lansdown, A.B. Silver in health care: Antimicrobial effects and safety in use. *Curr. Probl. Dermatol.* **2006**, *33*, 17–34. [CrossRef] [PubMed]
3. Nowack, B.; Krug, H.F.; Height, M. 120 years of nanosilver history: Implications for policy makers. *Environ. Sci. Technol.* **2011**, *45*, 1177–1183. [CrossRef] [PubMed]
4. Agnihotri, S.; Mukherji, S.; Mukherji, S. Size-controlled silver nanoparticles synthesized over the range 5-100 nm using the same protocol and their antibacterial efficacy. *RSC Adv.* **2014**, *4*, 3974–3983. [CrossRef]
5. Malalila, N.G.; Swai, H.S.; Hilonga, A.; Kadam, D.M. Antimicrobial dependence of silver nanoparticles on surface plasmon resonance bands against *Escherichia coli*. *Nanotechnol. Sci. Appl.* **2017**, *10*, 1–9. [CrossRef] [PubMed]
6. Yin, I.X.; Zhang, J.; Zhao, I.S.; Mei, M.L.; Li, Q.; Chu, C.H. The antibacterial mechanism of silver nanoparticles and its application in dentistry. *Int. J. Nanomed.* **2020**, *15*, 2555–2562. [CrossRef] [PubMed]
7. Jeremiah, S.S.; Miyakawa, K.; Morita, T.; Yamaoka, Y.; Ryo, A. Potent antiviral effect of silver nanoparticles on SARS-CoV-2. *Biochem. Biophys. Res. Commun.* **2020**, *533*, 195–200. [CrossRef] [PubMed]
8. Konradt, N.; Schneider, L.; Bianga, S.; Schroden, D.; Janknecht, P.; Krekel, G. Retention of Engineered Nanoparticles in Drinking Water Treatment Processes: Laboratory and Pilot-Scale Experiments. *Appl. Nano* **2024**, *5*, 279–310. [CrossRef]
9. Grand View Research. *Beta-Carotene Market Size, Share & Trends Analysis Report by Type (Natural, Synthetic), by End-Use (Food & Beverages, Pharmaceutical, Dietary Supplements), by Region (North America, Asia Pacific), And Segment Forecasts, 2024–2030*; Grand View Research: San Francisco, CA, USA, 2024.
10. Vanlalveni, C.; Lallianrawna, S.; Biswas, A.; Selvaraj, M.; Changmai, B.; Rokhum, S.L. Green synthesis of silver nanoparticles using plant extracts and their antimicrobial activities: A review of recent literature. *RSC Adv.* **2021**, *11*, 2804–2837. [CrossRef] [PubMed]
11. Burda, C.; Chen, X.; Narayanan, R.; El-Sayed, M.A. Chemistry and properties of nanocrystals of different shapes. *Chem. Rev.* **2005**, *105*, 1025–1102. [CrossRef] [PubMed]
12. Piszczek, P.; Radtke, A. Silver Nanoparticles Fabricated Using Chemical Vapor Deposition and Atomic Layer Deposition Techniques: Properties, Applications and Perspectives. In *Noble and Precious Metals—Properties, Nanoscale Effects and Applications*; Seehra, M.S., Bristow, A.D., Eds.; IntechOpen: London, UK, 2018; pp. 187–213.
13. Eker, F.; Akdasci, E.; Duman, H.; Bechelany, M.; Karav, S. Green synthesis of silver nanoparticles using plant extracts: A comprehensive review of physicochemical properties and multifunctional applications. *Int. J. Mol. Sci.* **2025**, *26*, 6222. [CrossRef] [PubMed]
14. Dunah, M.B.; Abdalla, M.A.; Wawata, I.G.; Adekilekun, T.N. Antibacterial activity of plant-extract mediated silver nanoparticles against *Klebsiella* spp. in Africa: A systematic review. *Front. Microbiol.* **2025**, *16*, 1673235. [CrossRef] [PubMed]
15. Khalifa, H.O.; Oreiby, A.; Mohammed, T.; Abdelhamid, M.A.A.; Sholkamy, E.N.; Hashem, H.; Fereig, R.M. Silver nanoparticles as next-generation antimicrobial agents: Mechanisms, challenges, and innovations against multidrug-resistant bacteria. *Front. Cell. Infect. Microbiol.* **2025**, *15*, 1599113. [CrossRef] [PubMed]
16. Jangid, H.; Joshi, H.C.; Dutta, J.; Ahmad, A.; Alshammari, M.B.; Hossain, K.; Pant, G.; Kumar, G. Advancing food safety with biogenic silver nanoparticles: Addressing antimicrobial resistance, sustainability, and commercial viability. *Food Chem. X* **2025**, *25*, 102298. [CrossRef] [PubMed]

17. Sati, A.; Ranade, T.N.; Mali, S.N.; Yasin, H.K.A.; Pratap, A. Silver nanoparticles (AgNPs): Comprehensive insights into bio/synthesis, key influencing factors, multifaceted applications, and toxicity—A 2024 update. *ACS Omega* **2025**, *10*, 7549–7582. [CrossRef] [PubMed]
18. Page, M.J.; McKenzie, J.E.; Bossuyt, P.M.; Boutron, I.; Hoffmann, T.C.; Mulrow, C.D.; Shamseer, L.; Tetzlaff, J.M.; Akl, E.A.; Brennan, S.E.; et al. The PRISMA 2020 statement: An updated guideline for reporting systematic reviews. *BMJ* **2021**, *372*, n71. [CrossRef] [PubMed]
19. Haynes, W.M. (Ed.) *CRC Handbook of Chemistry and Physics*, 97th ed.; CRC Press: Boca Raton, FL, USA, 2016.
20. Reidy, B.; Haase, A.; Luch, A.; Dawson, K.A.; Lynch, I. Mechanisms of silver nanoparticle release, transformation and toxicity: A critical review of current knowledge and recommendations for future studies and applications. *Materials* **2013**, *6*, 2295–2350. [CrossRef] [PubMed]
21. Nene, A.; Galluzzi, M.; Hongrong, L.; Somani, P.; Ramakrishna, S.; Yu, S.F. Synthetic preparations and atomic scale engineering of silver nanoparticles for biomedical applications. *Nanoscale* **2021**, *13*, 13923–13942. [CrossRef] [PubMed]
22. Subhan, A.; Ismail Mourad, A.H.; Al-Douri, Y. Influence of laser process parameters, liquid medium, and external field on the synthesis of colloidal metal nanoparticles using pulsed laser ablation in liquid: A review. *Nanomaterials* **2022**, *12*, 2144. [CrossRef] [PubMed]
23. Balachandran, A.; Sreenilayam, S.P.; Madanan, K.; Thomas, S.; Brabazon, D. Nanoparticle production via laser ablation synthesis in solution method and printed electronic application—A brief review. *Results Eng.* **2022**, *16*, 100646. [CrossRef]
24. Gamboa, S.M.; Rojas, E.R.; Martínez, V.V.; Vega-Baudrit, J. Synthesis and characterization of silver nanoparticles and their application as an antibacterial agent. *Int. J. Biosens. Bioelectron.* **2019**, *5*, 166–173. [CrossRef]
25. Morones, J.R.; Elechiguerra, J.L.; Camacho, A.; Holt, K.; Kouri, J.B.; Ramírez, J.T.; Yacaman, M.J. The bactericidal effect of silver nanoparticles. *Nanotechnology* **2005**, *16*, 2346–2353. [CrossRef] [PubMed]
26. Hamid, N.M.; Abed, H.A.; Fahad, O.A. Evaluation of antibacterial effects of silver nanoparticles synthesized via pulsed laser ablation at different laser energies. *Lasers Manuf. Mater. Process.* **2025**, *12*, 488–497. [CrossRef]
27. Pal, S.; Tak, Y.K.; Song, J.M. Does the antibacterial activity of silver nanoparticles depend on the shape of the nanoparticle? A study of the Gram-negative bacterium *Escherichia coli*. *Appl. Environ. Microbiol.* **2007**, *73*, 1712–1720. [CrossRef] [PubMed]
28. Levard, C.; Hotze, E.M.; Lowry, G.V.; Brown, G.E., Jr. Environmental transformations of silver nanoparticles: Impact on stability and toxicity. *Environ. Sci. Technol.* **2012**, *46*, 6900–6914. [CrossRef] [PubMed]
29. Liu, J.; Hurt, R.H. Ion release kinetics and particle persistence in aqueous nano-silver colloids. *Environ. Sci. Technol.* **2010**, *44*, 2169–2175. [CrossRef] [PubMed]
30. Kittler, S.; Greulich, C.; Diendorf, J.; Köller, M.; Epple, M. Toxicity of silver nanoparticles increases during storage because of slow dissolution under release of silver ions. *Chem. Mater.* **2010**, *22*, 4548–4554. [CrossRef]
31. Cakić, M.; Glišić, S.; Nikolić, G.; Nikolić, G.M.; Cakić, K.; Cvetinov, M. Synthesis, characterization and antimicrobial activity of dextran sulphate stabilized silver nanoparticles. *J. Mol. Struct.* **2016**, *1110*, 156–161. [CrossRef]
32. Sondi, I.; Salopek-Sondi, B. Silver nanoparticles as antimicrobial agent: A case study on *E. coli* as a model for Gram-negative bacteria. *J. Colloid Interface Sci.* **2004**, *275*, 177–182. [CrossRef] [PubMed]
33. Feng, Q.L.; Wu, J.; Chen, G.Q.; Cui, F.Z.; Kim, T.N.; Kim, J.O. A mechanistic study of the antibacterial effect of silver ions on *Escherichia coli* and *Staphylococcus aureus*. *J. Biomed. Mater. Res.* **2000**, *52*, 662–668. [CrossRef] [PubMed]
34. Yamanaka, M.; Hara, K.; Kudo, J. Bactericidal actions of a silver ion solution on *Escherichia coli*, studied by energy-filtering transmission electron microscopy and proteomic analysis. *Appl. Environ. Microbiol.* **2005**, *71*, 7589–7593. [CrossRef] [PubMed]
35. Xiu, Z.M.; Zhang, Q.B.; Puppala, H.L.; Colvin, V.L.; Alvarez, P.J.J. Negligible particle-specific antibacterial activity of silver nanoparticles. *Nano Lett.* **2012**, *12*, 4271–4275. [CrossRef] [PubMed]
36. Silver, S. Bacterial silver resistance: Molecular biology and uses and misuses of silver compounds. *FEMS Microbiol. Rev.* **2003**, *27*, 341–353. [CrossRef] [PubMed]
37. Gunawan, C.; Teoh, W.Y.; Marquis, C.P.; Amal, R. Induced adaptation of *Bacillus* sp. to antimicrobial nanosilver. *Small* **2013**, *9*, 3554–3560. [CrossRef] [PubMed]
38. Panáček, A.; Kvítek, L.; Smékalová, M.; Večeřová, R.; Kolář, M.; Röderová, M.; Dyčka, F.; Šebela, M.; Prucek, R.; Tomanec, O.; et al. Bacterial resistance to silver nanoparticles and how to overcome it. *Nat. Nanotechnol.* **2018**, *13*, 65–71. [CrossRef] [PubMed]
39. Randall, C.P.; Gupta, A.; Jackson, N.; Busse, D.; O'Neill, A.J. Silver resistance in Gram-negative bacteria: A dissociation between phenotype and genotype. *J. Antimicrob. Chemother.* **2015**, *70*, 1037–1046. [PubMed]
40. Shaheen, M.E.; Abdelwahab, A.Y.E. Laser ablation in liquids: A versatile technique for nanoparticle generation. *Opt. Laser Technol.* **2025**, *186*, 112705. [CrossRef]
41. Fernández-Arias, M.; Boutinguiza, M.; del Val, J.; Medina, E.; Rodríguez, D.; Riveiro, A.; Comesaña, R.; Lusquiños, F.; Gil, F.J.; Pou, J. Re-irradiation of silver nanoparticles obtained by laser ablation in water and assessment of their antibacterial effect. *Appl. Surf. Sci.* **2019**, *473*, 548–554. [CrossRef]

42. Menazea, A.A. Femtosecond laser ablation-assisted synthesis of silver nanoparticles in organic and inorganic liquids medium and their antibacterial efficiency. *Radiat. Phys. Chem.* **2020**, *168*, 108616. [CrossRef]
43. Ruiz, S.; Wang, F.; Liu, L.; Lu, Y.; Duan, B.; Korshoj, L.E.; Kielian, T.; Cui, B. Antibacterial properties of silver nanoparticles synthesized via nanosecond pulsed laser ablation in water. *J. Laser Appl.* **2022**, *34*, 012031. [CrossRef]
44. Pérez-Tanoira, R.; Fernández-Arias, M.; Potel, C.; Carballo-Fernández, R.; Pérez-Castro, S.; Boutinguiza, M.; Górgolas, M.; Lusquiños, F.; Pou, J. Silver nanoparticles produced by laser ablation and re-irradiation are effective preventing peri-implantitis multispecies biofilm formation. *Int. J. Mol. Sci.* **2022**, *23*, 12027. [CrossRef] [PubMed]
45. Abbas, R.H.; Haleem, A.M.; Kadhim, A. The antimicrobial effect of simultaneously applying different diode lasers and silver nanoparticles synthesized by laser ablation on bacterial dental caries. *Appl. Nanosci.* **2023**, *13*, 5589–5603. [CrossRef]
46. Manikandan, N.A.; McCann, R.; Kakavas, D.; Rochfort, K.D.; Sreenilayam, S.P.; Alkan, G.; Stornetta, T.; McGivern, A.R.; Grintzalis, K.; Friedrich, B.; et al. Production of silver nano-inks and surface coatings for anti-microbial food packaging and its ecological impact. *Int. J. Mol. Sci.* **2023**, *24*, 5341. [CrossRef] [PubMed]
47. Jaleh, B.; Mousavi, S.S.; Sajjadi, M.; Eslamipanah, M.; Maryaki, M.; Orooji, Y.; Varma, R.S. Synthesis of bentonite/Ag nanocomposite by laser ablation in air and its application in remediation. *Chemosphere* **2023**, *315*, 137668. [CrossRef] [PubMed]
48. Radtke, A.; Grodzicka, M.; Ehlert, M.; Jędrzejewski, T.; Wypij, M.; Golińska, P. "To be microbiocidal and not to be cytotoxic at the same time..."—Silver nanoparticles and their main role on the surface of titanium alloy implants. *J. Clin. Med.* **2019**, *8*, 334. [CrossRef] [PubMed]
49. Mäkelä, M.; Hatanpää, T.; Mizohata, K.; Meinander, K.; Niinistö, J.; Räisänen, J.; Ritala, M.; Leskelä, M. Studies on thermal atomic deposition of silver thin films. *Chem. Mater.* **2017**, *29*, 2040–2045. [CrossRef]
50. Wack, S.; Popa, P.L.; Adjeroud, N.; Guillot, J.; Pistillo, B.R.; Leturcq, R. Large-scale deposition and growth mechanism of silver nanoparticles by plasma-enhanced atomic layer deposition. *J. Phys. Chem. C* **2019**, *123*, 27196–27206. [CrossRef]
51. Devin-Mullin, A.; Todd, N.M.; Golrokhi, Z.; Geng, H.; Konerding, M.A.; Ternan, N.G.; Hunt, J.A.; Potter, P.J.; Sutcliffe, C.; Jones, E.; et al. Atomic layer deposition of a silver nanolayer on advanced titanium orthopaedic implants inhibits bacterial colonization and supports vascularized de novo bone ingrowth. *Adv. Healthc. Mater.* **2017**, *6*, 1700033. [CrossRef] [PubMed]
52. Gerullis, S.; Pfuch, A.; Spange, S.; Kettner, F.; Plaschkies, K.; Küzün, B.; Kosmachev, P.V.; Volokitin, G.G.; Grünler, B. Thin antimicrobial silver, copper or zinc containing SiOx films on wood polymer composites (WPC) applied by atmospheric pressure plasma chemical vapour deposition (APCVD) and sol-gel technology. *Eur. J. Wood Prod.* **2018**, *76*, 229–241. [CrossRef]
53. Astaneh, S.H.; Bhatia, H.; Nagay, B.E.; Barão, V.A.R.; Jursich, G.; Sukotjo, C.; Takoudis, C.G. Is atomic layer deposition of silver possible on N95 masks? *Appl. Surf. Sci.* **2022**, *591*, 153195. [CrossRef] [PubMed]
54. Nazarov, D.; Ezhov, I.; Yudintceva, N.; Shevtsov, M.; Rudakova, A.; Kalganov, V.; Tolmachev, V.; Zharova, Y.; Lutakov, O.; Kraeva, L.; et al. Antibacterial and osteogenic properties of Ag nanoparticles and Ag/TiO_2 nanostructures prepared by atomic layer deposition. *J. Funct. Biomater.* **2022**, *13*, 62. [CrossRef] [PubMed]
55. Chandana, L.; Ghosal, P.; Shashidhar, T.; Subrahmanyam, C. Enhanced photocatalytic and antibacterial activity of plasma-reduced silver nanoparticles. *RSC Adv.* **2018**, *8*, 24827–24835. [CrossRef] [PubMed]
56. Sun, D.; Turner, J.; Jiang, N.; Zhu, S.; Zhang, L.; Falzon, B.G.; Colin, P.; Maguire, P.; Mariotti, D.; Sun, D. Atmospheric pressure microplasma for antibacterial silver nanoparticle/chitosan nanocomposites with tailored properties. *Compos. Sci. Technol.* **2020**, *186*, 107911. [CrossRef]
57. da Silva, D.J.; Ferreira, G.S.; Duran, A.; Fonseca, F.L.A.; Bueno, R.F.; Rosa, D.S. Super effective antimicrobial silver-sputtered coatings on poly(lactic acid) against bacteria and omicron SARS-CoV-2. *Mater. Today Chem.* **2023**, *30*, 101481. [CrossRef]
58. Cook, A.L.; Haycook, C.P.; Locke, A.K.; Mu, R.; Giorgio, T.D. Optimization of electron beam-deposited silver nanoparticles on zinc oxide for maximally surface enhanced Raman spectroscopy. *Nanoscale Adv.* **2021**, *3*, 407–417. [CrossRef] [PubMed]
59. He, C.; Chen, Q.; Yarmolenko, M.A.; Rogachev, A.A.; Piliptsou, D.G.; Jiang, X.; Rogachev, A.V. Structure and antibacterial activity of PLA-based biodegradable nanocomposite coatings by electron beam deposition from active gas phase. *Prog. Org. Coat.* **2018**, *123*, 282–291. [CrossRef]
60. Gao, D.; Zhou, X.; Gao, Z.H.; Shi, X.; Wang, Z.; Wang, Y.; Zhang, P. Preparation and characterization of silver sulfadiazine loaded polyvinyl alcohol hydrogels as an antibacterial wound dressing. *J. Pharm. Sci.* **2018**, *107*, 2377–2384. [CrossRef] [PubMed]
61. Lampé, I.; Beke, D.; Biri, S.; Csarnovics, I.; Csik, A.; Dombrádi, Z.; Hajdu, P.; Hegedűs, V.; Rácz, R.; Varga, I.; et al. Investigation of silver nanoparticles on titanium surface created by ion implantation technology. *Int. J. Nanomed.* **2019**, *14*, 4709–4721. [CrossRef] [PubMed]
62. Kim, J.H.; Ma, J.; Jo, S.; Lee, S.; Kim, C.S. Enhancement of antibacterial properties of a silver nanowire film via electron beam irradiation. *ACS Appl. Bio Mater.* **2020**, *3*, 2117–2124. [CrossRef] [PubMed]
63. Chiangnoon, R.; Karawak, P.; Eamsiri, J.; Nuchdang, S.; Thamrongsiripak, N.; Neramitmansook, N.; Pummarin, S.; Pimton, P.; Nilgumhang, K.; Uttayarat, P. Antibacterial hydrogel sheet dressings composed of poly(vinyl alcohol) and silver nanoparticles by electron beam irradiation. *Gels* **2023**, *9*, 80. [CrossRef] [PubMed]
64. Granqvist, C.G.; Buhrman, R.A. Ultrafine metalparticles. *J. Appl. Phys.* **1976**, *47*, 2200–2219. [CrossRef]

65. Wada, N. Preparation of fine metal particles by the gas evaporation method with plasma jet flame. *Jpn. J. Appl. Phys.* **1969**, *8*, 551. [CrossRef]
66. Yatsuya, S.; Mihama, K.; Uyeda, R. A new technique for the preparation of extremely fine metal particles. *Jpn. J. Appl. Phys.* **1974**, *13*, 749–750. [CrossRef]
67. Akoh, H.; Tsukasaki, Y.; Yatsuya, S.; Tasaki, A. Magnetic properties of ferromagnetic ultrafine particles prepared by vacuum evaporation on running oil substrate. *J. Cryst. Growth* **1978**, *45*, 495–500. [CrossRef]
68. Matsuo, K.; Klabunde, K.J. Clustering of metal atoms in organic media: 9. High-activity Ni/MgO catalysts prepared by metal vapor methods. Surface area and particle size effects. *J. Catal.* **1982**, *73*, 216–227. [CrossRef]
69. Park, D.; Joe, Y.; Hwang, J.; Byeon, J.H. Evaporation-condensation in the presence of unipolar ionic flow for solvent-free production of ultrasmall antibacterial particles. *Chem. Eng. J.* **2020**, *381*, 122639. [CrossRef]
70. Sakono, N.; Shimizu, M.; Sakono, M. Immobilization method for silver nanoparticles synthesized via evaporation/condensation onto a glass plate. *Chem. Lett.* **2022**, *51*, 1074–1076. [CrossRef]
71. Vasil'kov, A.; Migulin, D.; Naumkin, A.; Volkov, I.; Butenko, I.; Golub, A.; Sadykova, V.; Muzafarov, A. Hybrid materials with antimicrobial properties based on hyperbranched polyaminopropylalkoxysiloxanes embedded with Ag nanoparticles. *Pharmaceutics* **2023**, *15*, 809. [CrossRef] [PubMed]
72. Seku, K.; Gangapuram, B.R.; Pejjai, B.; Kadimpati, K.K.; Golla, N. Microwave-assisted synthesis of silver nanoparticles and their application in catalytic, antibacterial and antioxidant activities. *J. Nanostruct. Chem.* **2018**, *8*, 179–188. [CrossRef]
73. Kumar, A.; Dalal, J.; Dahiya, S.; Punia, R.; Sharma, K.D.; Ohlan, A.; Maan, A.S. In situ decoration of silver nanoparticles on single-walled carbon nanotubes by microwave irradiation for enhanced and durable anti-bacterial finishing on cotton fabric. *Ceram. Int.* **2019**, *45*, 1011–1019. [CrossRef]
74. Araruna, F.B.; de Oliveira, T.M.; Quelemes, P.; de Araujo Nobre, A.R.; Plácido, A.; Vasconcelos, A.G.; Monteiro de Paulá, R.C.; Mafud, A.C.; de Almeida, M.P.; Delerue-Matos, C.; et al. Antibacterial application of natural and carboxymethylated cashew gum-based silver nanoparticles produced by microwave-assisted synthesis. *Carbohydr. Polym.* **2020**, *241*, 115260. [CrossRef] [PubMed]
75. Aljohani, M.M.; Abu-Rayyan, A.; Elsayed, N.H.; Alatawi, F.A.; Al-Anazi, M.; Mustafa, S.K.; Albalawi, R.K.; Abdelmonem, R. One-pot microwave synthesis of chitosan-stabilized silver nanoparticles entrapped polyethylene oxide nanofibers, with their intrinsic antibacterial and antioxidant potency for wound healing. *Int. J. Biol. Macromol.* **2023**, *235*, 123704. [CrossRef] [PubMed]
76. Mpala, T.J.; Serepa-Dlamini, M.H.; Etale, A.; Richards, H.; Nthunya, L.N. Cellulose nanocrystal-mediated synthesis of silver nanoparticles via microwave assisted method for biofouling control in membrane distillation. *Mater. Today Commun.* **2023**, *34*, 105028. [CrossRef]
77. García-Barrasa, J.; López-de-Luzuriaga, J.M.; Monge, M. Silver nanoparticles: Synthesis through chemical methods in solution and biomedical applications. *Cent. Eur. J. Chem.* **2011**, *9*, 7–19. [CrossRef]
78. Lee, P.C.; Meisel, D. Adsorption and surface-enhanced Raman of dyes on silver and gold sols. *J. Phys. Chem.* **1982**, *86*, 3391–3395. [CrossRef]
79. Creighton, J.A.; Blatchford, C.G.; Albrecht, M.G. Plasma resonance enhancement of Raman scattering by pyridine adsorbed on silver or gold sol particles of size comparable to the excitation wavelength. *J. Chem. Soc. Faraday Trans. 2* **1979**, *75*, 790–798. [CrossRef]
80. Yin, Y.; Li, Z.; Zhong, Z.; Gates, B.; Xia, Y.; Venkateswaran, S. Synthesis and characterization of stable aqueous dispersions of silver nanoparticles through the Tollens process. *J. Mater. Chem.* **2002**, *12*, 522–527. [CrossRef]
81. Thiruvengadam, V.; Bansod, A.V. Characterization of silver nanoparticles synthesized using chemical method and its antibacterial property. *Biointerface Res. Appl. Chem.* **2020**, *10*, 7257–7264. [CrossRef]
82. Mousavi-Khattat, M.; Keyhanfar, M.; Razmjou, A.A. A comparative study of stability, antioxidant, DNA cleavage and antibacterial activities of green and chemically synthesized silver nanoparticles. *Artif. Cells Nanomed. Biotechnol.* **2018**, *46*, 1022–1031. [CrossRef] [PubMed]
83. Sartori, P.; Delamare, A.P.L.; Machado, G.; Devine, D.M.; Crespo, J.S.; Giovanela, M. Synthesis and characterization of silver nanoparticles for the preparation of chitosan pellets and their application in industrial wastewater disinfection. *Water* **2023**, *15*, 190. [CrossRef]
84. Niu, Y.; Guo, T.; Yuan, X.; Zhao, Y.; Ren, L. Injectable supramolecular hydrogel hybridized with silver nanoparticles for antibacterial application. *Soft Matter* **2018**, *14*, 1227–1234. [CrossRef] [PubMed]
85. Sofia, N.G.; Nikos, B.; Elias, S.; Eleni, E.K. Synthesis of biocompatible silver nanoparticles by a modified polyol method for theranostic applications: Studies on red blood cells, internalization ability and antibacterial activity. *J. Inorg. Biochem.* **2020**, *211*, 111177. [CrossRef] [PubMed]
86. Mathew, S.; Snigdha, S.; Mathew, J.; Radhakrishnan, E.K. Poly(vinyl alcohol): Montmorillonite: Boiled rice water (starch) blend film reinforced with silver nanoparticles; characterization and antibacterial properties. *Appl. Clay Sci.* **2018**, *161*, 464–473. [CrossRef]

87. Muneeswaran, T.; Maruthupandy, M.; Mary, A.S.; Vennila, T.; Rajaram, K.; Ramakritinan, C.M.; Quero, F. Starch-mediated synthesis of chitosan/silver nanocomposites for antibacterial, antibiofilm and wound healing applications. *J. Drug Deliv. Sci. Technol.* **2023**, *84*, 104424. [CrossRef]
88. Vukoje, I.; Lazić, V.; Sredojević, D.; Fernandes, M.M.; Lanceros-Méndez, S.; Ahrenkiel, S.P.; Nedeljković, J.M. Influence of glucose, sucrose, and dextran coatings on the stability and toxicity of silver nanoparticles. *Int. J. Biol. Macromol.* **2022**, *194*, 461–469. [CrossRef] [PubMed]
89. Jatoi, A.W.; Kim, I.S.; Ni, Q.Q. A comparative study on synthesis of AgNPs on cellulose nanofibers by thermal treatment and DMF for antibacterial activities. *Mater. Sci. Eng. C* **2019**, *98*, 1179–1195. [CrossRef] [PubMed]
90. Lee, S.J.; Heo, M.; Lee, D.; Han, S.; Moon, J.H.; Lim, H.N.; Kwon, I.K. Preparation and characterization of antibacterial orthodontic resin containing silver nanoparticles. *Appl. Surf. Sci.* **2018**, *432*, 317–323. [CrossRef]
91. Althobaiti, F.; Abu Ali, O.A.; Kamal, I.; Alfaifi, M.Y.; Shati, A.A.; Fayad, E.; Elbehairi, S.E.I.; Elshaarawy, R.F.M.; El-Fattah, W.A. New ionic liquid microemulsion-mediated synthesis of silver nanoparticles for skin bacterial infection treatments. *Antibiotics* **2023**, *12*, 247. [CrossRef] [PubMed]
92. Amini, E.; Azadfallah, M. In situ synthesis of silver nanoparticles on fiber matrix for preparing antibacterial paper. *Biointerface Res. Appl. Chem.* **2018**, *8*, 3449–3456.
93. Begum, I.; Shamim, S.; Ameen, F.; Hussain, Z.; Bhat, S.A.; Qadri, T.; Hussain, M. A combinatorial approach towards antibacterial and antioxidant activity using tartaric acid capped silver nanoparticles. *Processes* **2022**, *10*, 716. [CrossRef]
94. Liao, S.; Zhang, Y.; Pan, X.; Zhu, F.; Jiang, C.; Liu, Q.; Cheng, Z.; Dai, G.; Wu, G.; Wang, L.; et al. Antibacterial activity and mechanism of silver nanoparticles against multidrug-resistant *Pseudomonas aeruginosa*. *Int. J. Nanomed.* **2019**, *14*, 1469–1487. [CrossRef] [PubMed]
95. Badineni, V.; Maseed, H.; Arla, S.K.; Yerramala, S.; Naidu, V.K.B.; Kaviyarasu, K. Effect of PVA/PVP protective agent on the formation of silver nanoparticles and its photocatalytic and antimicrobial activity. *Mater. Today Proc.* **2021**, *36*, 121–125. [CrossRef]
96. Wang, H.; Jiang, Y.; Zhang, Y.; Zhang, Z.; Yang, X.; Ali, M.A.; Fox, E.M.; Gobius, K.S.; Man, C. Silver nanoparticles: A novel antibacterial agent for control of *Cronobacter sakazakii*. *J. Dairy Sci.* **2018**, *101*, 10775–10791. [CrossRef] [PubMed]
97. Hileuskaya, K.; Ladutska, A.; Kulikouskaya, V.; Kraskouski, A.; Novik, G.; Kozerozhets, I.; Kozlovskiy, A.; Agabekov, V. Green' approach for obtaining stable pectin-capped silver nanoparticles: Physico-chemical characterization and antibacterial activity. *Colloids Surf. A Physicochem. Eng. Asp.* **2020**, *585*, 124141. [CrossRef]
98. Ibrahim, H.M.; Zaghloul, S.; Hashem, M.; El-Shafei, A. A green approach to improve the antibacterial properties of cellulose-based fabrics using *Moringa oleifera* extract in the presence of silver nanoparticles. *Cellulose* **2021**, *28*, 549–564. [CrossRef]
99. Alavi, M.; Karimi, N. Biosynthesis of Ag and Cu NPs by secondary metabolites of usnic acid and thymol with biological macromolecules aggregation and antibacterial activities against multidrug-resistant (MDR) bacteria. *Int. J. Biol. Macromol.* **2019**, *128*, 893–901. [CrossRef] [PubMed]
100. Guzmán, K.; Kumar, B.; Vallejo, M.J.; Grijalva, M.; Debut, A.; Cumbal, L. Ultrasound-assisted synthesis and antibacterial activity of gallic acid-chitosan modified silver nanoparticles. *Prog. Org. Coat.* **2019**, *129*, 229–235. [CrossRef]
101. Gangwar, C.; Yaseen, B.; Nayak, R.; Praveen, S.; Singh, N.K.; Sarkar, J.; Banerjee, M.; Naik, R.M. Silver nanoparticles fabricated by tannic acid for their antimicrobial and anticancerous activity. *Inorg. Chem. Commun.* **2022**, *141*, 109532. [CrossRef]
102. Tian, S.; Hu, Y.; Chen, X.; Liu, C.; Xue, Y.; Han, B. Green synthesis of silver nanoparticles using sodium alginate and tannic acid: Characterization and anti-*S. aureus* activity. *Int. J. Biol. Macromol.* **2022**, *195*, 515–522. [CrossRef] [PubMed]
103. Pisárčik, M.; Lukáč, M.; Jampílek, J.; Bilka, F.; Bilková, A.; Pašková, Ľ.; Devínsky, F.; Horáková, R.; Opravil, T. Phosphonium surfactant stabilised silver nanoparticles. Correlation of surfactant structure with physical properties and biological activity of silver nanoparticles. *J. Mol. Liq.* **2020**, *314*, 113683. [CrossRef]
104. Gibała, A.; Żeliszewska, P.; Gosiewski, T.; Krawczyk, A.; Duraczyńska, D.; Szaleniec, J.; Szaleniec, M.; Oćwieja, M. Antibacterial and antifungal properties of silver nanoparticles-effect of a surface-stabilizing agent. *Biomolecules* **2021**, *11*, 1481. [CrossRef] [PubMed]
105. Yu, D.; Yam, V.W.W. Controlled synthesis of monodisperse silver nanocubes in water. *J. Am. Chem. Soc.* **2004**, *126*, 13200–13201. [CrossRef] [PubMed]
106. Yu, D.; Yam, V.W.W. Hydrothermal-induced assembly of colloidal silver spheres into various nanoparticles on the basis of HTAB-modified silver mirror reaction. *J. Phys. Chem. B* **2005**, *109*, 5497–5503. [CrossRef] [PubMed]
107. Zielinska, A.; Skwarek, E.; Zaleska, A.; Gazda, M.; Hupka, J. Preparation of silver nanoparticles with controlled particle size. *Procedia Chem.* **2009**, *1*, 1560–1566. [CrossRef]
108. Monge, M. Silver nanoparticles: Synthesis methods in solution and bactericidal properties. *An. Quim.* **2009**, *105*, 33–41.
109. Yan, K.; Xu, F.; Wei, W.; Yang, C.; Wang, D.; Shi, X. Electrochemical synthesis of chitosan/silver nanoparticles multilayer hydrogel coating with pH-dependent controlled release capability and antibacterial property. *Colloids Surf. B Biointerfaces* **2021**, *202*, 111711. [CrossRef] [PubMed]

110. Zhang, J.; Xu, Q.; Li, H.; Zhang, S.; Hong, A.; Jiang, Y.; Hu, N.; Chen, G.; Fu, H.; Yuan, M.; et al. Triboelectric-nanogenerator-driven electrodeposition of silver nanoparticles with antibacterial effect. *J. Phys. Chem. Lett.* **2022**, *13*, 6721–6730. [PubMed]
111. Sudhisha, V.; Saranya, K.; Kalaiyarasan, M.; Rajendran, N. Silver nanoparticles doped poly(3,4-ethylenedioxythiophene) on titania nanotubes for orthopaedic application. *Appl. Surf. Sci.* **2023**, *610*, 155416. [CrossRef]
112. Calderón-Jiménez, B.; Montoro Bustos, A.R.; Pereira Reyes, R.; Paniagua, S.A.; Vega-Baudrit, J.R. Novel pathway for the sonochemical synthesis of silver nanoparticles with near-spherical shape and high stability in aqueous media. *Sci. Rep.* **2022**, *12*, 882. [CrossRef] [PubMed]
113. Andrade Neto, N.F.; Oliveira, Y.G.; Paskocimas, C.A.; Bomio, M.R.D.; Motta, F.V. Increase of antimicrobial and photocatalytic properties of silver-doped PbS obtained by sonochemical method. *J. Mater. Sci. Mater. Electron.* **2018**, *29*, 19052–19062. [CrossRef]
114. Sorinezami, Z.; Ghanbari, D. Facile preparation of silver nanoparticles and antibacterial chitosan-Ag polymeric nanocomposites. *J. Nanostruct.* **2019**, *9*, 396–401.
115. Tzounis, L.; Bangeas, P.I.; Exadaktylos, A.; Petousis, M.; Vidakis, N. Three-dimensional printed polylactic acid (PLA) surgical retractors with sonochemically immobilized silver nanoparticles: The next generation of low-cost antimicrobial surgery equipment. *Nanomaterials* **2020**, *10*, 985. [CrossRef] [PubMed]
116. Shepida, M.; Kuntyi, O.; Sozanskyi, M.; Sukhatskiy, Y. Sonoelectrochemical synthesis of antibacterial active silver nanoparticles in rhamnolipid solution. *Adv. Mater. Sci. Eng.* **2021**, *2021*, 7754523. [CrossRef]
117. Zozulya, G.; Kuntyi, O.; Mnykh, R.; Kytsya, A.; Bazylyak, L. Synthesis of silver nanoparticles by sonogalvanic replacement on aluminium powder in sodium polyacrylate solutions. *Ultrason. Sonochem.* **2022**, *84*, 105951. [CrossRef] [PubMed]
118. Abazari, M.; Badeleh, S.M.; Khaleghi, F.; Saeedi, M.; Haghi, F. Fabrication of silver nanoparticles-deposited fabrics as a potential candidate for the development of reusable facemasks and evaluation of their performance. *Sci. Rep.* **2023**, *13*, 1593. [CrossRef] [PubMed]
119. Courrol, D.D.S.; Lopes, C.R.B.; Cordeiro, T.D.S.; Franzolin, M.R.; Vieira Junior, N.D.; Samad, R.E.; Courrol, L.C. Optical properties and antimicrobial effects of silver nanoparticles synthesized by femtosecond laser photoreduction. *Opt. Laser Technol.* **2018**, *103*, 233–238. [CrossRef]
120. Van Viet, P.; Sang, T.T.; Bich, N.H.N.; Thi, C.M. An improved green synthesis method and *Escherichia coli* antibacterial activity of silver nanoparticles. *J. Photochem. Photobiol. B Biol.* **2018**, *182*, 108–114. [CrossRef] [PubMed]
121. Van Viet, P.; Phan, B.T.; Mott, D.; Maenosono, S.; Sang, T.T.; Thi, C.M.; Hieu, L.V. Silver nanoparticle loaded TiO_2 nanotubes with high photocatalytic and antibacterial activity synthesized by photoreduction method. *J. Photochem. Photobiol. A Chem.* **2018**, *352*, 106–112. [CrossRef]
122. Paiva, L.; Fidalgo, T.K.S.; da Costa, L.P.; Maia, L.C.; Balan, L.; Anselme, K.; Ploux, L.; Thiré, R.M.S.M. Antibacterial properties and compressive strength of new one-step preparation silver nanoparticles in glass ionomer cements (NanoAg-GIC). *J. Dent.* **2018**, *69*, 102–109. [CrossRef] [PubMed]
123. Villanueva, M.E.; Ghibaudo, M.F.; Tovar, G.I.; Copello, G.J.; Campo Dall'Orto, V. Oligomer-stabilized silver nanoparticles for antimicrobial coatings for plastics. *Nano-Struct. Nano-Objects* **2020**, *24*, 100610. [CrossRef]
124. Dong, S.; Hua, H.; Wu, X.; Mao, X.; Li, N.; Zhang, X.; Wang, K.; Yang, S. In-situ photoreduction strategy for synthesis of silver nanoparticle-loaded PVDF ultrafiltration membrane with high antibacterial performance and stability. *Environ. Sci. Pollut. Res.* **2023**, *30*, 26445–26457. [CrossRef] [PubMed]
125. Poudel, M.B.; Kim, A.A. Silver nanoparticles decorated TiO_2 nanoflakes for antibacterial properties. *Inorg. Chem. Commun.* **2023**, *152*, 110675. [CrossRef]
126. Mittal, A.K.; Bhattacharya, A.; Chisti, Y.; Banerjee, U.C. Biosynthesis of silver nanoparticles: Elucidation of prospective mechanism and therapeutic potential. *J. Colloid Interface Sci.* **2014**, *415*, 39–47. [CrossRef] [PubMed]
127. Mittal, A.K.; Chisti, Y.; Banerjee, U.C. Synthesis of metallic nanoparticles using plant extracts. *Biotechnol. Adv.* **2013**, *31*, 346–356. [CrossRef] [PubMed]
128. Haefeli, C.; Franklin, C.; Hardy, K. Plasmid-determined silver resistance in *Pseudomonas stutzeri* isolated from a silver mine. *J. Bacteriol.* **1984**, *158*, 389–392. [CrossRef] [PubMed]
129. Bhaumik, J.; Thakur, N.S.; Aili, P.K.; Ghanghoriya, A.; Mittal, A.K.; Banerjee, U.C. Bioinspired nanotheranostic agents: Synthesis, surface functionalization, and antioxidant potential. *ACS Biomater. Sci. Eng.* **2015**, *1*, 382–392. [CrossRef] [PubMed]
130. Ahmed, S.; Ahmad, M.; Swami, B.L.; Ikram, S. A review on plants extract mediated synthesis of silver nanoparticles for antimicrobial applications: A green expertise. *J. Adv. Res.* **2016**, *7*, 17–28. [CrossRef] [PubMed]
131. Kesharwani, J.; Yoon, K.Y.; Hwang, J.; Rai, M. Phytofabrication of silver nanoparticles by leaf extract of Datura metel: Hypothetical mechanism involved in synthesis. *J. Bionanosci.* **2009**, *3*, 39–44. [CrossRef]
132. Thakur, N.S.; Dwivedee, B.P.; Banerjee, U.C.; Bhaumik, J. Bioinspired synthesis of silver nanoparticles: Characterisation, mechanism and applications. In *Silver Nanoparticles for Antibacterial Devices: Biocompatibility and Toxicity*; Cao, H., Ed.; Taylor & Francis/CRC Press: Boca Raton, FL, USA, 2017.

133. Makarov, V.V.; Love, A.J.; Sinitsyna, O.V.; Makarova, S.S.; Yaminsky, I.V.; Taliansky, M.E.; Kalinina, N.O. "Green" nanotechnologies: Synthesis of metal nanoparticles using plants. *Acta Nat.* **2014**, *6*, 35–44. [CrossRef]
134. Dakshayani, S.S.; Marulasiddeshwara, M.B.; Sharath Kumar, M.N.; Golla, R.; Raghavendra Kumar, P.; Devaraja, S.; Hosamani, R. Antimicrobial, anticoagulant and antiplatelet activities of green synthesized silver nanoparticles using *Selaginella* (Sanjeevini) plant extract. *Int. J. Biol. Macromol.* **2019**, *131*, 787–797. [CrossRef] [PubMed]
135. Pirtarighat, S.; Ghannadnia, M.; Baghshahi, S. Green synthesis of silver nanoparticles using the plant extract of *Salvia spinosa* grown in vitro and their antibacterial activity assessment. *J. Nanostruct. Chem.* **2019**, *9*, 1–9. [CrossRef]
136. Mohammed, A.E.; Al-Qahtani, A.; Al-Mutairi, A.; Al-Shamri, B.; Aabed, K. Antibacterial and cytotoxic potential of biosynthesized silver nanoparticles by some plant extracts. *Nanomaterials* **2018**, *8*, 382. [CrossRef] [PubMed]
137. Díaz-Puertas, R.; Álvarez-Martínez, F.J.; Rodríguez-Cañas, E.; Borrás, F.; Valente, A.J.M.; Paixao, J.A.; Falcó, A.; Mallavia, R. An innovative approach based on the green synthesis of silver nanoparticles using pomegranate peel extract for antibacterial purposes. *Bioinorg. Chem. Appl.* **2025**, *2025*, 2009069. [CrossRef] [PubMed]
138. Khorrami, S.; Kamali, F.; Zarrabi, A. Bacteriostatic activity of aquatic extract of black peel pomegranate and silver nanoparticles biosynthesized by using the extract. *Biocatal. Agric. Biotechnol.* **2020**, *25*, 101620. [CrossRef]
139. Reda, M.; Ashames, A.; Edis, Z.; Bloukh, S.; Bhandare, R.; Abu Sara, H. Green synthesis of potent antimicrobial silver nanoparticles using different plant extracts and their mixtures. *Processes* **2019**, *7*, 510. [CrossRef]
140. Nayak, P.S.; Pradhan, S.; Arakha, M.; Kumar, D.; Saleem, M.; Mallick, B.; Jha, S. Silver nanoparticles fabricated using medicinal plant extracts show enhanced antimicrobial and selective cytotoxic propensities. *IET Nanobiotechnol.* **2019**, *13*, 193–201. [CrossRef] [PubMed]
141. Chahar, B.; Sharma, G.; Srivastava, A.; Bhatnagar, A. Study of antimicrobial activity of silver nanoparticles synthesized using green and chemical approach. *Colloids Surf. A* **2018**, *554*, 149–155. [CrossRef]
142. Farouk, S.M.; Abu-Hussien, S.H.; Abd-Elhalim, B.T.; Mohamed, R.M.; Arabe, N.M.; Hussain, A.A.T.; Mostafa, M.E.; Hemdan, B.; El-Sayed, S.M.; Bakry, A.; et al. Biosynthesis and characterization of silver nanoparticles from *Punica granatum* (pomegranate) peel waste and its application to inhibit foodborne pathogens. *Sci. Rep.* **2023**, *13*, 19469. [CrossRef] [PubMed]
143. Mafhala, L.; Khumalo, N.; Zikalala, N.E.; Azizi, S.; Cloete, K.J.; More, G.K.; Kamika, I.A.; Mokrani, T.; Zinatizadeh, A.A.; Maaza, M. Antibacterial and cytotoxicity activity of green synthesized silver nanoparticles using aqueous extract of naartjie (*Citrus unshiu*) fruit peels. *Emerg. Contam.* **2024**, *10*, 100348. [CrossRef]
144. Hani, U.; Kidwan, F.N.; Albarqi, L.A.; Al-qahtani, S.A.; AlHadi, R.M.; AlZaid, H.A.; Haider, N.; Ansari, M.A. Biogenic silver nanoparticle synthesis using orange peel extract and its multifaceted biomedical application. *Bioprocess Biosyst. Eng.* **2024**, *47*, 1363–1375. [CrossRef] [PubMed]
145. AshaRani, P.V.; Low Kah Mun, G.; Hande, M.P.; Valiyaveettil, S. Cytotoxicity and genotoxicity of silver nanoparticles in human cells. *ACS Nano* **2009**, *3*, 279–290. [CrossRef] [PubMed]
146. Kim, S.; Choi, J.E.; Choi, J.; Chung, K.H.; Park, K.; Yi, J.; Ryu, D.Y. Oxidative stress-dependent toxicity of silver nanoparticles in human hepatoma cells. *Toxicol. Vitr.* **2009**, *23*, 1076–1084. [CrossRef] [PubMed]
147. Marambio-Jones, C.; Hoek, E.M.V. A review of the antibacterial effects of silver nanomaterials and potential implications for human health and the environment. *J. Nanopart. Res.* **2010**, *12*, 1531–1551. [CrossRef]

Disclaimer/Publisher's Note: The statements, opinions and data contained in all publications are solely those of the individual author(s) and contributor(s) and not of MDPI and/or the editor(s). MDPI and/or the editor(s) disclaim responsibility for any injury to people or property resulting from any ideas, methods, instructions or products referred to in the content.